Differentiation in the photo-protective mechanism of the Light Harvesting Complex stress-related proteins LHCX1 and LHCX2 of the marine diatom *Phaeodactylum tricornutum*

Abstract

In diatoms, the expression of the Light Harvesting Complex (LHCX) gene family is closely related to Non-Photochemical Quenching (NPQ) responses, which serve significant photoprotective functions under fluctuating or high light conditions. Previous studies of the LHCX gene expression dynamics highlighted the function of LHCX1 in modulating NPQ, and several hypotheses describing the structural role of LHCX1 in the fucoxanthin chlorophyll-a/c pigment protein complex (FCPC) have been proposed to justify the connection between LHCX1 and NPQ. Based on these previous findings, we further investigated the role of LHCX1 in facilitating photo-acclimation by comparing the photophysiology and transcriptomic responses in wild type (WT) and LHCX1 knockout lines under low light and 24 hour high light acclimation conditions. The results indicate that LHCX1 regulates NPQ upon FCPC aggregation induced by high light stress, and the level of NPQ is dependent on the aggregation states. Moreover, we found that the rate of LHCX2 induced NPQ is more rapid than LHCX1, indicating the response of NPQ due to LHCX2 might be faster than FCPC aggregation. LHCX1 knockouts caused *P. tricornutum* to establish a different acclimation state after 24 hour high light treatment, with lower photosynthetic efficiencies caused by acceleration of NPQ as a result of LHCX2 induction combined with down regulation of ribosomal protein expression. The study of LHCX genes provides important insight into the role of NPQ in regulating energy transfer during high light acclimation.

Introduction

Light is the ultimate energy source for photosynthesis and the subsequent cell growth of microalgae. However, excess light can cause damage to the photosynthetic apparatus and even result in cell death (Raven, 2011). Through evolution microalgae have evolved a variety of photoprotective mechanisms including: non-photochemical quenching (NPQ), alternative electron transport that redistributes energy between photosystem I and II (PSI and PSII), and D1 protein damage-repair (Horton & Ruban, 2005; Nymark *et al.*, 2009; Raven, 2011). Among them, NPQ is the protective mechanism that is most capable of responding to sudden irradiance increases, dissipating excess energy as heat via molecular vibration (Peers, 2014). The discovery by Peers *et al.* (2009) first unveiled the significance of an ancient Light Harvesting Complex Stress Related protein (LHCX) in regulating NPQ response in *Chlamydomonas*. Soon after that, members of the LHCX family were discovered in the marine diatom *Phaeodactylum tricornutum*, and the transcription levels of LHCX1, LHCX2 and LHCX3 were found to be dependent on light intensity (Bailleul *et al.*, 2010; Lepetit *et al.*, 2013). Interestingly, the genes encoding these proteins are absent in higher plants (Neilson & Durnford, 2010), indicating that the LHCX family is related to NPQ regulation under the frequently shifting light conditions that are common for aquatic microalgae. In diatoms, the fucoxanthin chlorophyll-a/c protein complex (FCPC) functions as the light harvesting comple. In *P. tricornuntum* the basic unit of the FCPC protein complex is trimeric, as it is in the chlorophyll-a/b light harvesting complex (LHC) in green algae and higher plants (Lepetit *et al.*, 2007). FCPC proteins are encoded by three group of genes that include the LHCX family, which was hypothesized to be essential for the structural change in the light harvesting complex during the induction of NPQ measured by chlorophyll a fluorescence (Wilhelm *et al.*, 2014).

The FCPC contains a high concentration of fucoxanthin (Fx) pigment, which serves as the main light-harvesting accessory pigment. Fx is biosynthetically associated with the xanthophyll cycle (XC) pigments, while the ratio of Fx to XC pigments depends on the photo-acclimation state (Wilhelm *et al.*, 2014). For high light acclimation, the diatom *Cyclotella meneghiniana*, was found to have a fast and strongly pH dependent NPQ response during the slower conversion of diadinoxanthin (Ddx) to diatoxanthin (Dtx) Grouneva *et al.* (2009). Gundermann & Büchel (2012) further proposed a FCPC regulated NPQ model, in which the FCPC units are spread out under dark or low light (LL) conditions. With increased light intensity, these units first aggregate to form a more packed complex with decreased fluorescence yield. This may be related to increased NPQ under most conditions; however the change in absorption related to both a smaller absorption cross-section (Miloslavina *et al.*, 2009) and possibly lower absorption per unit pigment from pigment packaging effects (Morel & Bricaud, 1981; Mitchell & Kiefer, 1988) must be taken into account as well. This aggregation phenomenon was confirmed experimentally with isolated FCPC from *P. tricornutum* (Schaller-Laudel *et al.*, 2015). FCPC aggregation can reduce fluorescence yield by up to 85% even without XC (Grouneva *et al.,* 2009). By global transcriptional profiling, Nymark *et al.* (2009) found that three of the four LHCX genes (LHCX 1-3) were up-regulated immediately after the high light treatment was applied. Further investigation of LHCX genes by Bailleul *et al.* (2010) showed LHCX1 expression is closely related to the NPQ capacity. However, LHCX1 expression was not significantly up regulated under high light treatment. In addition, Bailleul *et al.* (2010) also found the lack of LHCX1 protein is not associated with a diminished XC, suggesting its involvement in protective mechanism is not through direct NPQ induction, but possibly through functioning as a molecular gauge controlling the level of NPQ from XC.

LHCX1 has been shown to modulate NPQ capacity during a typical light/dark cycle and transgenic RNAi knockdown lines with inhibited LHCX1 expression have significantly reduced NPQ and growth rates (Bailleul et al., 2010). However, the mechanism for how LHCX1 regulates NPQ remains unclear because some of the observed experimental data do not support previously hypothesized LHCX1 functions. The measured NPQ strongly corresponds to the expression level of LHCX1, but the level of LHCX1 expression is not up regulated with increasing light intensity. The de-expoxidation state (DES) of XC is independent of the level of LHCX1 expression, suggesting LHCX1 is not always the key enzyme that regulates NPQ and it is not involved in the XC. Additionally, the measured PSII cross-section and oxygen evolution rate did seem not to be affected by the inhibition of LHCX1 expression, leading us to speculate that LHCX1 may not be a structural protein in FCPC under all conditions. In this study we seek to characterize the role of LHCX1 in photosynthesis and photoacclimation in *P. tricornutum.*

Materials and Methods

Knocking out the LHCX1 gene in *Phaeodactylum tricornutum*

We used Crispr-Cas9 genome editing to enable bi-allelic homologous recombination of the Sh-ble gene, a zeocin antibiotic-resistance marker, into a double-strand break to generate *P. tricornutum* LHCX1 knockout lines. We selected 3 transgenic lines that showed disrupted LHCX1 gene loci from a pool of transformed cell lines, and picked one of the transgenic lines (named LHCX1A) for detailed experiments. (Details of the knockout methods and related validations are in supporting information)

Cultivation and environmental control

The *P. tricornutum* wild type strain CCAP1055/1 (McCarthy et al., 2017) and our LHCX1A knockout line were cultured in triplicates with Artificial Sea Water medium (ASW; www3.botany.ubc.ca/cccm/NEPCC/esaw.html) contained in 175ml sterile VWR polystyrene tissue culture flasks. Cultures were maintained at 25 °C in Percival incubators, under 24 hours illumination supplied by a white LED source. A light diffuser was installed for light homogenization and heat isolation. Each flask with 125ml culture volume was laid horizontally on top of the light diffuser to maximize the surface area for illumination and to minimize light attenuation in the vertical direction. Cultures were diluted semi-continuously to keep their optical density at 750nm, below 0.2 in order to avoid nutrient and carbon limitation and to reduce cell shading. The culture light intensity was initially set at 110 μmol photons m^{-2} s^{-1} (LL), and cells were grown for more than 6 division cycles (~3 days) to enable sufficient acclimation before shifting to 750 μmole quanta m^{-2} s^{-1} light (HL), for the 24 hours acclimation experiment. Detailed physiological experiments were conducted at the beginning and the end of the experiment. During the HL period samples were taken at time 0, 1, 3, 6, 12 and 24 hour time points for simultaneous carbon uptake and oxygen evolution quantum yields (Φ_C, Φ_{O2}) measurement, with the use of a pHOS-MIMS system and a spectral photometer equipped with an integrating sphere. In addition, scalar irradiance (Photosynthetically Active Radiation, 400–700 nm) in the culture flasks was measured with a Li-Cor irradiance sensor with a 4 π probe, and relative spectral irradiance was measured with a Newport portable spectrophotometer equipped with an integrating sphere.

Chlorophyll a-specific absorption coefficient

In vivo whole cell absorption was determined at 1 nm intervals from 400-700 nm using a dual beam spectrophotometer (Cary 100) equipped with a 30 cm Lab Sphere integrating sphere

(Moisan & Mitchell, 1999). The chlorophyll a-specific spectral absorption coefficient $a^*_{ph}(\lambda)$ is defined as:

$$a^*_{ph}(\lambda) = \frac{a_{ph}(\lambda)}{[Chl\,a]} \qquad \text{Equation 4.1}$$

Chlorophyll a concentration was measured on 90% acetone extracts after 24 hours at 4°C using a Turner 10-AU fluorometer calibrated with pure chlorophyll a (Sigma).

Quantum yield (Φ) calculation

The calculation of Φ (mole carbon or oxygen / mole photons absorbed) for both carbon uptake and oxygen evolution using the definition of net growth, modified from Sosik and Mitchell (1991) (Equation 2). Where P is the rate of net photosynthesis (O_2 evolution or CO_2 fixation) and the spectral integration of the product $a^*_{ph}(\lambda)$ and spectral irradiance $E_0(\lambda)$ is the total photon flux absorbed by the culture.

$$\phi = \frac{P}{\int_{400\,nm}^{700\,nm} a^*_{ph}(\lambda) E_0(\lambda)\, d\lambda} \qquad \text{Equation 4.2}$$

Particulate carbon and nitrogen (POC/PON)

For POC and PON estimates, a 10 ml sample was filtered onto a 0.2 μm Nuclepore polycarbonate filter under vacuum pressure < 5 PSI. The concentrated biomass was then washed into a 25 ml acid-washed TOC glass vial with 20 ml DI water. A blank was determined by filtering an equal volume of DI water and then processing it identically to the other samples. The samples and blanks were then analyzed with a Shimadzu TOC-L Analyzer using the total carbon and nitrogen (TC/TN) protocol, and the final POC and PON results were determined by

subtracting the measurement values from the blank.

P vs. E

Samples re-suspended in ASW medium with known alkalinity were inoculated into the glass cell of an ALGI^{TM} with the integrated pH oscillation (pHOS) and membrane inlet mass-spectrometer (MIMS) system for simultaneous pH and dissolved oxygen and argon measurements (Chapter 3). The cell mixing, light and temperature control for the measurement was achieved by the ALGI^{TM} system that has been validated previously (Meuser *et al.*, 2011; Noone *et al.*, 2017). During measurement, samples were exposed to alternating dark/light periods with 2 min intervals and at increasing light intensity steps of 0, 20, 50, 200, 500, 1000, and 2000 μmole quanta m^{-2} s^{-1}. Measurement of the pH and O_2/Ar ratio were recorded at 1 Hz during the dark/light periods for computing DIC and O_2 concentrations. The rate of both parameters measured during the first dark period (light intensity = 0 μmole m^{-2} s^{-1}) and the following light periods were used to create the P vs. E curves. For the curve fitting we offset the respiration rate to force the data to start at 0 so we could use the Platt et al. (1980) function because this calculation does not allow the use of negative values. The offset respiration value was then subtracted from the fitted result following Richardson et al. (1983).

RNAseq and Harvesting

RNAseq samples were collected at the beginning and the end of the 24 hour HL acclimation treatment for both WT and LHCX1A cell lines. The biological triplicated samples were aliquoted in 50mL Falcon tubes. Depending on cell density, samples collected for RNA were filtered on 5.0 uM SVPP Durapore filters (Millipore Sigma) then flash frozen in liquid nitrogen and stored at −80° C until needed. RNA was extracted using Trizol Reagent (Thermo

Fisher Scientific), genomic DNA was removed with DNase I (TURBO DNA-free™ Kit, ThermoFisher Scientific), followed by RNA purification with the Agencourt RNAClean XP beads (Beckman Coulter). RNA samples were enriched for mRNA using NEBNext® Poly(A) mRNA Magnetic Isolation Module (New England Biolabs). Libraries were constructed using ScriptSeq v2 RNA-Seq kit (Illumina), library quality verified on the Agilent 2200 TapeStation System and sequencing of 66 libraries was run on the Illumina Single-Read 50 (SR50) platform.

Sequence-Read Mapping Paired-end

Paired-end Illumina HiSeq reads were quality trimmed to Phred score 33 and at least 30 bp in length. Filtered reads were mapped to contigs of *P. tricornutum* (http://genome.jgi.doe.gov/Phatr2/Phatr2.home.html) using HISAT2 (Kim *et al.*, 2015). Raw read counts and TPMs for genes were based on Phatr3 gene models (http://protists.ensembl.org/Phaeodactylum_tricornutum/Info/Index).

Transcriptome Analysis

Differential expression analysis was performed using Python3.6 in Jupyter notebook (Robinson et al., 2010) on raw read counts to obtain transcript per million (TPM ; Li & Dewey, 2011) and normalized fold changes. The PCA analysis was conducted using Python 3.6 with the scikit-learn library (Pedregosa *et al.*, 2012). Expression profiles of individual genes and gene clusters were developed using an AD HOC artificial neural network (ANN) designed for this dataset (Figure 7; supporting information).

Results

Photophysiology dynamics resulting from LHCX1 knockout in *P. tricornutum*

The reduced NPQ response in LHCX1A compared to WT at the beginning (0 hour) of LL-to-HL acclimation confirmed this phenotype (Figure 4.1). After 24 hours of HL, the NPQ response in the WT dropped roughly by 50% but in the LHCX1A line it increased by more than 100%, and the maximal NPQ level in LHCX1A exceeded WT. We found the rate of change in WT NPQ slowed down between 50 and 100 seconds. This two-stage response in WT after 24 hour HL acclimation might be caused by the reduced rate of FCPC aggregation, which resulted from protonation of the antenna protein and de-epoxidation of diadinoxanthin to diatoxanthin. Notably, the NPQ response at 0 hours did not exhibit this trend. The FCPC aggregation is known to induce strong energy dissipation as NPQ (Goss & Jakob, 2010). As the cells reach a HL acclimation state after 24 hours, the reduced cell specific photon absorption (Figure 4.2) can slow down the accumulation of the proton gradient required for protonation, causing the NPQ to rise after 100s (Figure 4.1; WT 0 hour). The LHCX1A line has almost identical cell specific absorption as the WT at 0 hour, but higher Chla specific absorption (Figure 4.2). This suggests the pigment in LHCX1A is less affected by the packaging effect. The overall energy input at the cellular level in both lines at 0 hours are similar, and similar growth rates were observed in both lines. This is possible because NPQ under LL condition can be quite low, and therefore the difference in NPQ capacity is not noticeable. LHCX1A NPQ increased much faster than WT at 24 hours during the entire measurement period, indicating a different NPQ response mechanism. At 0 hours, values of Fv/Fm in both the WT and LHCX1A lines were approximately 0.7, indicating that cells were close to their maximal photosynthetic capacity. After 24 hours, a significant drop in Fv/Fm was found in both lines, as a result of HL stress and consequent

photoinhibition, and this effect was found to be more severe in the LHCX1A line. The differences at time 0 and 24 hours in cellular Chla concentrations, POC/Chla, particulate carbon and nitrogen (POC/PON) (Table 1) are consistent with previous published studies on *P. tricornutum* acclimated to different light conditions (Costa et al., 2013), thus confirming that the detected physiological changes in both cell lines are correlated to the HL acclimation and stress responses. The increased cellular carbon and nitrogen levels after 24 hours of high light is consistent with observations by Anning et al. (2000) for *Skeletonenum costatum*, for a similar low to high light experiment and changes in the C/Chla ratio is consistent with many previous research results for microalgae (Falkowski & Raven, 2013)

Photosynthesis vs. irradiance (P vs. E) responses (Figure 4.3) and the Chla specific absorption coefficient (Figure 4.2) were used to determine the dynamics of the maximum quantum yield (Φ_{max}) for both carbon uptake and oxygen evolution during the 24 hour HL acclimation period. At 0 hour, Chla specific oxygen evolution and carbon uptake rates in LHCX1A were slightly higher than the WT when exposed to > 500 μmole photons m^{-2} s^{-1} measurement light. At 24 hour, the shift of P vs. E response in WT culture is consistent with previous studies on the diatom *Skeletonema costatum* at 50 and 1200 μmole quanta m^{-2} s^{-1}, respectively (Anning et al., 2000). Compared to WT, after 24 hours both oxygen evolution and carbon uptake rates in the LHCX1A line were lower for all light levels in the P vs. E curve (Figure 4.3). From the calculated Φ vs E we estimated the maximal quantum yields Φ_{max} and the corresponding light intensities where the maximum occurred (Figure 4.4). In the WT line, the observed Φ_{max} dropped significantly during the LL-to-HL acclimation because both the Chla-specific absorption and also the light intensity corresponding to the Φ_{max} increased significantly during acclimation (Figure 4.2). Compared to WT, Φ_{max} for both carbon and oxygen in the

LHCX1A line was slightly lower at 0 hour, and had a large drop after 3 hours. Another noticeable difference with the shift to high light was the strong increase in the light intensity where Φ_{max} was attained for both oxygen evolution and carbon uptake in the LHCX1A line, although after 24 hours the light intensities for carbon uptake Φ_{max} were similar in both lines (Figure 4.4).

WT and LHCX1A gene expressions during LL to HL acclimation

RNA-Seq assays were conducted for all triplicated WT and LHCX1A cell lines at 0 and 24 hour time points of the acclimation experiment. The Poly(A) captured cDNA library sequencing results were mapped to a referenced genome ASM15095v2 from Ensembl that included 10,402 gene models. TPM was then calculated for the raw counts and 10,054 genes with average counts >10 were selected for further analysis. Principle component analysis (PCA) was performed on the processed TPM data. These results showed the expressions of WT and LHCX1A at 0 hour are much more similar than at 24 hours (Figure 4.5). The light acclimation (related to PC1) contributed more to the variance in differential expressions than the knockout of LHCX1; the knockout had less variance and was related to PC2. Based on the PCA result and TPM data, we designed 7 expression types to represent possible trends observed in our RNA-Seq results (Figure 4.6). Types 1-5 describe patterns in which WT and LHCX1A have similar expression levels at 0 hour; types 6 and 7 describe patterns where WT and LHCX1A are different regardless of the light treatment. Patterns of WT and LHCX1A with reversed expression trend (expression increased in WT but decreased in LHCX1A due to HL, and vice versa) were rarely observed from a quick data survey; therefore, they were not included in the classification. We calculated the geometric mean of TPM for each gene model and defined three features for classification (Supporting information). By conducting selections using these three

features and their relationship to each other, we selected 1148 genes from the total of 10054 genes that satisfy the criteria that we chose for expression pattern classification without overlapping, and we then used these genes and their corresponding one hot encoding binary result for training an artificial neural network (ANN).

The training dataset was relatively small and the input layer has only one vector with four scalars; therefore, we designed the ANN to contain one hidden layer and one output layer to minimize the architecture complexity and subsequently reduce the time needed for hypo-parameter optimization (Figure 4.6). For this specific study, we randomly picked 50% of the samples from the selected genes for training and the other 50% for model validation. A dropout function with 0.8 keep rate was applied to the hidden layer to avoid over-fitting of the training data set, while the learning rate was set to a default value of 0.1 in Tensorflow. We analyzed the performance of this model with different hidden layer sizes and found the cost function minimized and converged after 10,000 iterations for all models tested. Additionally, both the error rates for training and validation sets decreased following power laws as the size of hidden layer increased and reached minimal levels when the size exceeded 100 nodes. We set the hidden layer size to 300 nodes for better performance; the additional computing power for the additional 200 nodes does not add much additional computation time in this simple model.

Although the properly defined and trained ANN model with the selected dataset minimized bias and variance within, when applying it for predicting the remaining dataset the variance of prediction can still be high because features extracted for those genes are more similar to each other, consequently small variations in the trained model parameters can have large impacts on the classification results. Thus, we performed a bootstrap aggregation with 100 random sub-samples to improve the stability of the ANN model prediction, and the final

classification result was based on the highest voting. The trained ANN model was then used to classify 4854 *P. tricornutum* genes that have Clusters of Orthologous Groups (COGs; Tatusov 2000) annotated functions, and the classified genes were normalized to their corresponding functional groups to show the relative density distribution of expression types (Figure 4.8). Based on the density distribution results, we calculated the connectivity of all annotated functional groups plus one 'Control' group to represent scenarios with no difference between WT and LHCA1A expression. The calculation of correlation was based on the signed weighted gene co-expression network analysis (WGCNA) method (Zhang & Horvath, 2005), and the similarity of expression patterns among functional groups were shown as distances between nodes in Figure 4.8. Among the 23 functional groups (including an unknown group) annotated in COGs, 3 exhibited contrasting expression patterns compared to the control and other groups.

Discussion

LHCX1, a light harvesting complex stress-related gene in *P. tricornutum*, is highly expressed under LL acclimated condition and the level of its product is known to directly affect NPQ response for a given amount of Dtx synthesized (Bailleul *et al.*, 2010; Lepetit *et al.*, 2013, 2017). Previous studies on LHCX1 have focused on its role in regulating NPQ. For example, the inhibited LHCX1 expression and subsequent lower protein accumulation was found to reduce NPQ capacity (Bailleul *et al.*, 2010; Lepetit *et al.*, 2013, 2017). The measured NPQ at the 0 hour time point supports previous findings showing the lack of LHCX1 significantly reduced NPQ levels in the LHCX1A line compared to WT. After 24 hours of LL-to-HL acclimation, the NPQ in WT decreased as a result of reduced light harvesting per reaction center and the number of reaction centers per cell due to photoacclimation (Falkowski & Raven, 2013). The increased NPQ response in the LHCX1A line after 24 hour acclimation has not been found in previous

literature; the closest observation was by Bailleul *et al.* (2010), in which the LL acclimated WT and LHCX1 knockdown line were exposed to HL for 1 hour before taking the second NPQ measurement, and the results showed a slight increase of NPQ in both lines. However, this observation might be an artifact of the increased pigment biosynthesis due to higher energy input during the initial stage of LL-to-HL acclimation (Ritz & Thomas, 2000) which would result in increased light absorption leading to higher NPQ, and may not be related to transcriptional regulation associated with longer-term acclimation. Our results indicate that the increased NPQ in LHCX1A line is related to LHCX2 function, and the hypothesis is supported by the transcriptomic data in which the transcription of LHCX2 in the LHCX1A line has more than a 6 fold increase (Figure 4.10). *P. tricornutum* WT under LL acclimation has a high rate of NPQ, however for HL acclimation the WT has lower concentrations of light harvesting pigments and during NPQ induction this lowers the rate of light absorption, resulting in slower formation of a proton gradient, leading to slower aggregation and a low rate of NPQ (Miloslavina *et al.*, 2009; Goss & Jakob, 2010). Previous results are consistent with the WT data from our experiments. Compared to WT, the NPQ response in the LHCX1A line sampled after 24 hour HL acclimation continued to increase without plateauing between 50-100 s. The two-phase response in WT is possibly a result of slower FCPC aggregation, which is essential for the LHCX1 protein to induce NPQ dissipation (Goss & Jakob, 2010). We speculate that the LHCX2 forms a permanent bond either to the xanthophyll pigments or to part of the protein complex very close to the xanthophyll pigments allowing rapid induction of NPQ under HL acclimated conditions, regardless of the aggregation state (Figure 4.11).

The observed photoacclimation physiology, including cellular carbon and nitrogen concentrations, Fv/Fm, and Chla specific oxygen evolution P vs. E, showed no observable

difference between WT and LHCX1A lines at the 0 hour time point, except cellular Chla concentration was slightly higher in the WT. Importantly, the cell specific absorption coefficient data show no observable difference between WT and LHCX1A at 0 hours. These findings support the model that LHCX1 is involved in FCPC aggregation (Goss & Jakob, 2010) rather than the hypothesis of a structural role in *P. tricornutum* (Bailleul *et al.*, 2010; Zhu & Green, 2010). The transcriptomic results show that LHCX1 is the predominently expressed gene among the LHCX family under LL condition, which is consistent with results shown in previous literature (Bailleul *et al.*, 2010; Lepetit *et al.*, 2013). Compared to time 0 (LL acclimation), signficant changes in cell composition were found in both WT and LHCX1A lines after 24 hour HL acclimation however no major differences were found between WT and LHCX1A lines. However, the photophysioslogy dynamcies including Fv/Fm, oxygen evolution and carbon uptake P vs E and quantum yields suggest that the LHCX1A line is more severely photo-inhibited at 24 hours.

Relative expression based neural network analysis (NNA), predicts photosynthesis and ribosomal biosynthesis are the two most severely affected functions as a result of HL stress when NPQ induction from LHCX1 is lacking during LL-to-HL acclimation. Within the photosynthesis functional group, type 2 expression genes predicted from the NNA are the same group of genes (Figure 4.12) that showed upregulation under HL stress in Nymark *et al.* (2009). For the "Translation, ribosomal structure and biogenesis" group, 34% and 29% of the gene expressions belong to type 3 and 4, and in "RNA processing and modification" group, 17 and 33% of the gene expressions belong to to type 3 and 4, respectively. These data provide clear evidence that for the LHCX1A line, HL stress related light harvesting protein expressions are up regulated to provide additional photoprotection and acclimation in response to HL. These genes

include some of the LHCR family members that are associated with PSI alternative electron transport function (Lepetit *et al.*, 2013), and LHCX2 and LHCX3 that are related to NPQ. The reduced ribosomal biosynthesis expressions are in agreement with the reduced chlorophyll specific carbon uptake and oxygen evolution rates in the LHCX1A line when compared to the WT line after 24 hour high light acclimation, indicating inhibited biosynthesis of key enzymes in chloroplast electron transport and in the CBB cycle. Interestly, photodamage repair related genes, FTSH, HCF136 and PSB27 (Figure 4.13; Nymark *et al.*, 2009), are not significantly up regulated in the LHCX1A line compared to WT, suggesting photodamage is not a significant factor causing reduced photosynthesis in the LHCX1A line.

Conclusions

Our study supports the interpretation that LHCX1 has an important role in regulating NPQ under HL and dynamic light conditons in *P. tricornutum* proposed in previous literature (Bailleul *et al.*, 2010; Lepetit *et al.*, 2013), and highlights the role of LHCX1 in LL-to-HL acclimation. With the LHCX1 function knocked out, *P. tricornutum* can still acclimate to HL, however the achieved acclimation state was quite different from the WT. The measured NPQ response suggests that the LHCX1 function was activated upon HL exposure together with FCPC aggregation. LHCX2 can replace some LHCX1 functions, however LHCX2 induced more rapid NPQ responses, suggesting the mechanisms of NPQ induction by LHCX1 and LHCX2 are different. Without sufficient NPQ protection from LHCX1 during high light stress and acclimation, the cells had a greater biosynthetic investment in energy dissipation and alternative electron transport, and down regulated other essential functions in photosynthesis. The combined result was the loss of energy from harvested photons and consequently inhibited oxygen evolution and carbon fixation. Nevertheless, this inhibition did not seem to be related to

photodamage; instead a stress related transcriptomic regulation is hypothesized to be responsible for the inefficient energy transfer.

References

Aalderink R, Jovin R. **1997**. Estimation of the photosynthesis/irradiance (P/I) curve parameters from light and dark bottle experiments. *Journal of plankton research* **19**: 1713–1742.

Abida H, Dolch L-J, Meï C, Villanova V, Conte M, Block MA, Finazzi G, Bastien O, Tirichine L, Bowler C. 2015. Membrane glycerolipid remodeling triggered by nitrogen and phosphorus starvation in Phaeodactylum tricornutum. *Plant physiology* **167**: 118–36.

Allen AE, LaRoche J, Maheswari U, Lommer M, Schauer N, Lopez PJ, Finazzi G, Fernie AR, Bowler C. **2008**. Whole-cell response of the pennate diatom Phaeodactylum tricornutum to iron starvation. *Proceedings of the National Academy of Sciences* **105**: 10438–10443.

Allen ED, Spence DHN. **1981**. the Differential Ability of Aquatic Plants To Utilize the Inorganic Carbon Supply in Fresh Waters. *New Phytologist* **87**: 269–283.

Anning T, MacIntyre HL, Pratt SM, Sammes PJ, Gibb S, Geider RJ. **2000**. Photoacclimation in the marine diatom *Skeletonema costatum*. *Limnology and Oceanography* **45**: 1807–1817.

Archibald JM. **2015**. Endosymbiosis and eukaryotic cell evolution. *Current Biology* **25**: R911–R921.

Aro EM, McCaffery S, Anderson JM. **1993**. Photoinhibition and D1 Protein Degradation in Peas Acclimated to Different Growth Irradiances. *Plant Physiology* **103**: 835–843.

Bailleul B, Berne N, Murik O, Petroutsos D, Prihoda J, Tanaka A, Villanova V, Bligny R, Flori S, Falconet D. 2015. Energetic coupling between plastids and mitochondria drives CO2 assimilation in diatoms. *Nature* **524**: 366–369.

Bailleul B, Rogato A, de Martino A, Coesel S, Cardol P, Bowler C, Falciatore A, Finazzi G. **2010**. An atypical member of the light-harvesting complex stress-related protein family modulates diatom responses to light. *Proceedings of the National Academy of Sciences* **107**: 18214–18219.

Bannister TT. **1979**. Quantitative description of steady state, nutrient-saturated algal growth, including adaptation. *Limnology and Oceanography* **24**: 76–96.

Bauwe H, Hagemann M, Fernie AR. **2010**. Photorespiration: players, partners and origin. *Trends in Plant Science* **15**: 330–336.

Bauwe H, Hagemann M, Kern R, Timm S. **2012**. Photorespiration has a dual origin and manifold links to central metabolism. *Current Opinion in Plant Biology* **15**: 269–275.

Behrenfeld MJ, Falkowski PG. **1997**. A consumer's guide to phytoplankton primary productivity models. *Limnology and Oceanography* **42**: 1479–1491.

Biello D. **2013**. Can Algae Feed the World and Fuel the Planet ? A Q & A with Craig Venter.

Scientific American: 1–6.

Bordbar A, Yurkovich JT, Paglia G, Rolfsson O, Sigurjónsson ÓE, Palsson BO. **2017**. Elucidating dynamic metabolic physiology through network integration of quantitative time-course metabolomics. *Scientific Reports* **7**: 46249.

Brewer PG, Goldman JC. **1976**. Alkalinity changes generated by phytoplankton growth1. *Limnology and Oceanography* **21**: 108–117.

Broddrick JT, Rubin BE, Welkie DG, Du N, Mih N, Diamond S, Lee JJ, Golden SS, Palsson BO. **2016**. Unique attributes of cyanobacterial metabolism revealed by improved genome-scale metabolic modeling and essential gene analysis. *Proceedings of the National Academy of Sciences* **113**: E8344–E8353.

Brzezowski P, Richter AS, Grimm B. **2015**. Regulation and function of tetrapyrrole biosynthesis in plants and algae. *Biochimica et Biophysica Acta (BBA) - Bioenergetics* **1847**: 968–985.

Chauton MS, Winge P, Brembu T, Vadstein O, Bones AM. **2013**. Gene Regulation of Carbon Fixation, Storage, and Utilization in the Diatom Phaeodactylum tricornutum Acclimated to Light/Dark Cycles. *Plant Physiology* **161**: 1034–1048.

Corcoran AA, Van Voorhies WA. **2012**. Simultaneous measurements of oxygen and carbon dioxide fluxes to assess productivity in phytoplankton cultures. *Journal of Microbiological Methods* **91**: 377–379.

Corps C. **2011**. Chapter 16: Memories of changes in renal care over three decades - The human perspective on registry statistics. *Nephron - Clinical Practice* **119**: 191.

Dambek M, Eilers U, Breitenbach J, Steiger S, Büchel C, Sandmann G. **2012**. Biosynthesis of fucoxanthin and diadinoxanthin and function of initial pathway genes in Phaeodactylum tricornutum. *Journal of Experimental Botany* **63**: 5607–5612.

Davis A, Abbriano R, Smith SR, Hildebrand M. **2017**. Clarification of Photorespiratory Processes and the Role of Malic Enzyme in Diatoms. *Protist* **168**: 134–153.

Dekker JP, Boekema EJ. **2005**. Supramolecular organization of thylakoid membrane proteins in green plants. *Biochimica et Biophysica Acta*: 12–39.

DelValls TA, Dickson AG. **1998**. The pH of buffers based on 2-amino-2-hydroxymethyl-1,3-propanediol ('tris') in synthetic sea water. *Deep-Sea Research Part I: Oceanographic Research Papers* **45**: 1541–1554.

Demmig-Adams B, Adams WW. **1996**. The role of xanthophyll cycle carotenoids in the protection of photosynthesis. *Trends in Plant Science* **1**: 21–26.

Dickson AG. **1984**. pH scales and proton-transfer reactions in saline media such as sea water. *Geochimica et Cosmochimica Acta* **48**: 2299–2308.

Domingues N, Matos AR, da Silva JM, Cartaxana P. **2012**. Response of the Diatom Phaeodactylum tricornutum to photooxidative stress resulting from high light exposure. *PLoS ONE* **7**: 1–6.

Dubinsky Z, Stambler N. **2009**. Photoacclimation processes in phytoplankton: Mechanisms, consequences, and applications. *Aquatic Microbial Ecology* **56**: 163–176.

Dyrssen D. **1965**. A Gran Titration of Sea Water on Board Sagitta. *Acta Chemica Scandinavica* **19**: 1265–1265.

Ebrahim A, Lerman JA, Palsson BO, Hyduke DR. **2013**. COBRApy: COnstraints-Based Reconstruction and Analysis for Python. *BMC Systems Biology* **7**: 74.

Eisenhut M, Ruth W, Haimovich M, Bauwe H, Kaplan A, Hagemann M. **2008**. The photorespiratory glycolate metabolism is essential for cyanobacteria and might have been conveyed endosymbiontically to plants. *Proceedings of the National Academy of Sciences* **105**: 17199–17204.

Falkowski PG, Chen Y-B. **2003**. Photoacclimation of Light Harvesting Systems in Eukaryotic Algae. In: Light-Harvesting Antennas in Photosynthesis Advances in Photosynthesis and Respiration Volume 13. 423–447.

Falkowski PG, LaRoche J. **1991**. Acclimation to spectral irradiance in algae. *Journal of Phycology* **27**: 8–14.

Falkowski PG, Owens TG. **1980**. Light--Shade Adaptation : two strategies in marine phytoplankton. *Plant physiology* **66**: 592–595.

Falkowski PG, Raven JA. **2013**. *Aquatic photosynthesis*. Princeton University Press.

Fawley MW. **1984**. Effects of Light Intensity and Temperature Interactions on Growth Characteristics of Phaeodactylum Tricornutum (Bacillariophyceae). *Journal of Phycology* **20**: 67–72.

Fischer G, Shah M, N. Tubiello F, van Velhuizen H. **2005**. Socio-economic and climate change impacts on agriculture: an integrated assessment, 1990-2080. *Philosophical Transactions of the Royal Society B: Biological Sciences* **360**: 2067–2083.

Fisher T, Berner T, Iluz D, Dubinsky Z. **1998**. The kinetics of the photoacclimation response of Nannochloropsis sp. (Eustigmatophyceae): A study of changes in ultrastructure and PSU density. *Journal of Phycology* **34**: 818–824.

Flori S, Jouneau P-H, Bailleul B, Gallet B, Estrozi LF, Moriscot C, Bastien O, Eicke S, Schober A, Bártulos CR. 2017. Plastid thylakoid architecture optimizes photosynthesis in diatoms. *Nature Communications* **8**: 15885.

Foyer CH, Noctor G. **2009**. Redox Regulation in Photosynthetic Organisms: Signaling, Acclimation, and Practical Implications. *Antioxidants & Redox Signaling* **11**: 861–905.

Garcia HE, Gordon LI. **1992**. Oxygen Solubility Sin Seawater: Better Fitting Equations. *Limnology and Oceanography* **37**: 1307–1312.

Ge F, Huang W, Chen Z, Zhang C, Xiong Q, Bowler C, Yang J, Xu J, Hu H. **2014**. Methylcrotonyl-CoA Carboxylase Regulates Triacylglycerol Accumulation in the Model Diatom Phaeodactylum tricornutum. *The Plant Cell* **26**: 1681–1697.

Geider RJ, Osborne BA, Raven JA, Osbonie BA, Raven JA. **1986**. Growth, photosynthesis and maintenance metabolic cost in the diatom Phaeodactylum tricornutum at very low light levels. *Journal of Phycology* **22**: 39–48.

Geiderl RJ, Maclntyre HL, Kana TM. **1998**. A dynamic regulatory model of phytoplanktonic acclimation to light, nutrients, and temperature. *Limnol. Oceanogr* **43**: 679–694.

Genty B, Briantais JM, Baker NR. **1989**. The relationship between the quantum yield of photosynthetic electron transport and quenching of chlorophyll fluorescence. *Biochimica et Biophysica Acta - General Subjects* **990**: 87–92.

Goss R, Ann Pinto E, Wilhelm C, Richter M. **2006**. The importance of a highly active and ΔpH-regulated diatoxanthin epoxidase for the regulation of the PS II antenna function in diadinoxanthin cycle containing algae. *Journal of Plant Physiology* **163**: 1008–1021.

Goss R, Jakob T. **2010**. Regulation and function of xanthophyll cycle-dependent photoprotection in algae. *Photosynthesis Research* **106**: 103–122.

Goss R, Wilhelm C. **2009**. Lipids in algae, lichens and mosses. *Lipids in Photosynthesis : Essential and Regulatory Functions*: 117–135.

Goussias C, Boussac A, Rutherford AW. **2002**. Photosystem II and photosynthetic oxidation of water: an overview. *Philosophical Transactions of the Royal Society B: Biological Sciences* **357**: 1369–1381.

Green BR, Durnford DG. **1996**. the Chlorophyll-Carotenoid Proteins of Oxygenic Photosynthesis. *Annual Review of Plant Physiology and Plant Molecular Biology* **47**: 685–714.

Greg Mitchell B, Kiefer DA. **1988**. Chlorophyll α specific absorption and fluorescence excitation spectra for light-limited phytoplankton. *Deep Sea Research Part A. Oceanographic Research Papers* **35**: 639–663.

Grossman AR, Schaefer MR, Chiang GG, Collier JL. **1993**. The phycobilisome, a light-harvesting complex responsive to environmental conditions. *Microbiological reviews* **57**: 725–49.

Grouneva I, Jakob T, Wilhelm C, Goss R. **2009**. The regulation of xanthophyll cycle activity and of non-photochemical fluorescence quenching by two alternative electron flows in the diatoms Phaeodactylum tricornutum and Cyclotella meneghiniana. *Biochimica et Biophysica Acta - Bioenergetics* **1787**: 929–938.

Grouneva I, Rokka A, Aro EM. **2011**. The thylakoid membrane proteome of two marine diatoms outlines both diatom-specific and species-specific features of the photosynthetic machinery. *Journal of Proteome Research* **10**: 5338–5353.

Gundermann K, Büchel C. **2012**. Factors determining the fluorescence yield of fucoxanthin-chlorophyll complexes (FCP) involved in non-photochemical quenching in diatoms. *Biochimica et Biophysica Acta - Bioenergetics* **1817**: 1044–1052.

Hakala M, Tuominen I, Keränen M, Tyystjärvi T, Tyystjärvi E. **2005**. Evidence for the role of the oxygen-evolving manganese complex in photoinhibition of Photosystem II. *Biochimica et Biophysica Acta - Bioenergetics* **1706**: 68–80.

Halsey KH, O'Malley RT, Graff JR, Milligan AJ, Behrenfeld MJ. **2013**. A common partitioning strategy for photosynthetic products in evolutionarily distinct phytoplankton species. *New Phytologist* **198**: 1030–1038.

Havurinne V, Tyystjärvi E. **2017**. Action Spectrum of Photoinhibition in the Diatom Phaeodactylum tricornutum. *Plant and Cell Physiology* **58**: 2217–2225.

Hernández-Ayon JM, Zirino A, Dickson a. G, Camiro-Vargas T, Valenzuela E. **2007**. Estimating the contribution of organic bases from microalgae to the titration alkalinity in coastal seawaters. *Limnology and Oceanography: Methods* **5**: 225–232.

Hiscock MR, Lance VP, Apprill AM, Bidigare RR, Johnson ZI, Mitchell BG, Smith WO, Barber RT. **2008**. Photosynthetic maximum quantum yield increases are an essential component of the Southern Ocean phytoplankton response to iron. *Proceedings of the National Academy of Sciences of the United States of America* **105**: 4775–4780.

Hoegh-Guldberg O, Mumby PJ, Hooten AJ, Steneck RS, Greenfield P, Gomez E, Harvell CD, Sale PF, Edwards AJ, Caldeira K. 2007. Coral reefs under rapid climate change and ocean acidification. *Science (New York, N.Y.)* **318**: 1737–1742.

Hopkinson BM, Dupont CL, Allen AE, Morel FMM. **2011a**. Efficiency of the CO2-concentrating mechanism of diatoms. *Proceedings of the National Academy of Sciences* **108**: 3830–3837.

Hopkinson BM, Dupont CL, Allen AE, Morel FMM. **2011b**. Efficiency of the CO2-concentrating mechanism of diatoms. *Proceedings of the National Academy of Sciences of the United States of America* **108**: 3830–7.

Horton P, Ruban A. **2005**. Molecular design of the photosystem II light-harvesting antenna: Photosynthesis and photoprotection. *Journal of Experimental Botany* **56**: 365–373.

Hunsperger HM, Ford CJ, Miller JS, Cattolico RA. **2016**. Differential regulation of duplicate light-dependent protochlorophyllide oxidoreductases in the diatom Phaeodactylum tricornutum (A Ianora, Ed.). *PLoS ONE* **11**: e0158614.

Imramovsky A, Pesko M, Ferriz JM, Kralova K, Vinsova J, Jampilek J. **2011**.

Photosynthesis - Inhibiting efficiency of 4-chloro-2- (chlorophenylcarbamoyl)phenyl alkylcarbamates. *Bioorganic and Medicinal Chemistry Letters* **21**: 4564–4567.

Jakob T, Wagner H, Stehfest K, Wilhelm C. **2007**. A complete energy balance from photons to new biomass reveals a light- and nutrient-dependent variability in the metabolic costs of carbon assimilation. *Journal of Experimental Botany* **58**: 2101–2112.

Jallet D, Caballero MA, Gallina AA, Youngblood M, Peers G. **2016**. Photosynthetic physiology and biomass partitioning in the model diatom Phaeodactylum tricornutum grown in a sinusoidal light regime. *Algal Research* **18**: 51–60.

Jones F. **2010**. Quantum Mechanics in Photosynthesis. : 1–6.

Kazmierczak J, Altermann W. **2002**. Neoarchean biomineratization by benthic cyanobacteria. *Science* **298**: 2351.

Keele BB, McCord JM, Fridovich I. **1970**. Superoxide Dismutase from Escherichia coli B: a new manganese-containing enzyme. *Journal of Biological Chemistry* **245**: 6176–6181.

Keeling CD, Whorf TP, Wahlen M, van der Plichtt J. **1995**. Interannual extremes in the rate of rise of atmospheric carbon dioxide since 1980. *Nature* **375**: 666–670.

Kiefer D a., Mitchell BG. **1983**. A simple steady state description of phytoplankton growth based on absorption cross section and quantum efficiency. *Limnology and Oceanography* **28**: 770–776.

Kim D, Langmead B, Salzberg SL. **2015**. HISAT: A fast spliced aligner with low memory requirements. *Nature Methods* **12**: 357–360.

Kromkamp JC, Forster RM. **2003**. The use of variable fluorescence measurements in aquatic ecosystems: Differences between multiple and single turnover measuring protocols and suggested terminology. *European Journal of Phycology* **38**: 103–112.

Kroth PG, Chiovitti A, Gruber A, Martin-Jezequel V, Mock T, Parker MS, Stanley MS, Kaplan A, Caron L, Weber T. 2008. A Model for Carbohydrate Metabolism in the Diatom Phaeodactylum tricornutum Deduced from Comparative Whole Genome Analysis. *PLoS ONE* **3**: e1426.

Krüger TPJ, Malý P, Alexandre MTA, Mančal T, Büchel C, Van R. **2017**. How reduced excitonic coupling enhances light harvesting in the main photosynthetic antennae of diatoms.

Kuczynska P, Jemiola-Rzeminska M, Strzalka K. **2015**. Photosynthetic pigments in diatoms. *Marine Drugs* **13**: 5847–5881.

Laws EA, Bannister TT. **1980**. Nutrient- and light-limited growth of Thalassiosira fluviatilis in continuous culture, with implications for phytoplankton growth in the ocean1. *Limnology and Oceanography* **25**: 457–473.

Lepetit B, Gélin G, Lepetit M, Sturm S, Vugrinec S, Rogato A, Kroth PG, Falciatore A, Lavaud J. **2017**. The diatom Phaeodactylum tricornutum adjusts nonphotochemical fluorescence quenching capacity in response to dynamic light via fine-tuned Lhcx and xanthophyll cycle pigment synthesis. *New Phytologist* **214**: 205–218.

Lepetit B, Goss R, Jakob T, Wilhelm C. **2012**. Molecular dynamics of the diatom thylakoid membrane under different light conditions. *Photosynthesis Research* **111**: 245–257.

Lepetit B, Sturm S, Rogato A, Gruber A, Sachse M, Falciatore A, Kroth PG, Lavaud J. **2013**. High Light Acclimation in the Secondary Plastids Containing Diatom Phaeodactylum tricornutum is Triggered by the Redox State of the Plastoquinone Pool. *Plant Physiology* **161**: 853–865.

Lepetit B, Volke D, Szabó M, Hoffmann R, Garab G, Wilhelm C, Goss R. **2007**. Spectroscopic and molecular characterization of the oligomeric antenna of the diatom Phaeodactylum tricornutum. *Biochemistry* **46**: 9813–9822.

Levering J, Broddrick J, Dupont CL, Peers G, Beeri K, Mayers J, Gallina AA, Allen AE, Palsson BO, Zengler K. **2016**. Genome-scale model reveals metabolic basis of biomass partitioning in a model diatom. *PLoS ONE* **11**: 1–22.

Li B, Dewey CN. **2011**. RSEM: Accurate transcript quantification from RNA-Seq data with or without a reference genome. *BMC Bioinformatics* **12**.

Lohr M, Wilhelm C. **2001**. Xanthophyll synthesis in diatoms: Quantification of putative intermediates and comparison of pigment conversion kinetics with rate constants derived from a model. *Planta* **212**: 382–391.

MacIntyre HL, Kana TM, Anning T, Geider RJ. **2002**. Photoacclimation of photosynthesis irradiance response curves and photosynthetic pigments in microalgae and cyanobacteria. *Journal of Phycology* **38**: 17–38.

Malviya S, Scalco E, Audic S, Vincent F, Veluchamy A, Poulain J, Wincker P, Iudicone D, de Vargas C, Bittner L. 2016. Insights into global diatom distribution and diversity in the world's ocean. *Proceedings of the National Academy of Sciences* **113**: E1516–E1525.

McCarthy JK, Smith SR, McCrow JP, Tan M, Zheng H, Beeri K, Roth R, Lichtle C, Goodenough U, Bowler CP. 2017. Nitrate Reductase Knockout Uncouples Nitrate Transport from Nitrate Assimilation and Drives Repartitioning of Carbon Flux in a Model Pennate Diatom. *The Plant Cell* **29**: 2047–2070.

Mehler AH. **1951**. Studies on reactions of illuminated chloroplasts. I. Mechanism of the reduction of oxygen and other Hill reagents. *Archives of biochemistry and biophysics* **33**: 65–77.

Meuser JE, Boyd ES, Ananyev G, Karns D, Radakovits R, Murthy UMN, Ghirardi ML, Dismukes GC, Peters JW, Posewitz MC. **2011**. Evolutionary significance of an algal gene encoding an [FeFe]-hydrogenase with F-domain homology and hydrogenase activity in Chlorella variabilis NC64A. *Planta* **234**: 829–843.

Miloslavina Y, Grouneva I, Lambrev PH, Lepetit B, Goss R, Wilhelm C, Holzwarth AR. **2009**. Ultrafast fluorescence study on the location and mechanism of non-photochemical quenching in diatoms. *Biochimica et Biophysica Acta - Bioenergetics* **1787**: 1189–1197.

Moisan TA, Ellisman MH, Buitenhuys CW, Sosinsky GE. **2006**. Differences in chloroplast ultrastructure of Phaeocystis antarctica in low and high light. *Marine Biology* **149**: 1281–1290.

Moisan TA, Mitchell BG. **1999**. Photophysiological acclimation of Phaeocystis antarctica Karsten under light limitation. *Limnology and oceanography* **44**: 247–258.

Morel A. **1978**. Available, usable, and stored radiant energy in relation to marine photosynthesis. *Deep-Sea Research* **25**: 673–688.

Morel A, Bricaud A. **1981**. Theoretical results concerning light absorption in a discrete medium, and application to specific absorption of phytoplankton. *Deep Sea Research Part A, Oceanographic Research Papers* **28**: 1375–1393.

Munekage Y, Hashimoto M, Miyake C, Tomizawa KI, Endo T, Tasaka M, Shikanai T. **2004**. Cyclic electron flow around photosystem I is essential for photosynthesis. *Nature* **429**: 579–582.

Nawrocki WJ, Tourasse NJ, Taly A, Rappaport F, Wollman F-A. **2015**. The Plastid Terminal Oxidase: Its Elusive Function Points to Multiple Contributions to Plastid Physiology. *Annual Review of Plant Biology* **66**: 49–74.

Neilson JAD, Durnford DG. **2010**. Structural and functional diversification of the light-harvesting complexes in photosynthetic eukaryotes. *Photosynthesis Research* **106**: 57–71.

Nelson N, Ben-Shem A. **2004**. The complex architecture of oxygenic photosynthesis. *Nature Reviews Molecular Cell Biology* **5**: 971–982.

Nixon PJ, Barker M, Boehm M, De Vries R, Komenda J. **2005**. FtsH-mediated repair of the photosystem II complex in response to light stress. *Journal of Experimental Botany* **56**: 357–363.

Nixon PJ, Michoux F, Yu J, Boehm M, Komenda J. **2010**. Recent advances in understanding the assembly and repair of photosystem II. *Annals of Botany* **106**: 1–16.

Niyogi KK. **1999**. Photoprotection revisited: *Genetic and Molecular Approaches*. *Annual Review of Plant Physiology and Plant Molecular Biology* **50**: 333–359.

Noone S, Ratcliff K, Davis RA, Subramanian V, Meuser J, Posewitz MC, King PW, Ghirardi ML. **2017**. Expression of a clostridial [FeFe]-hydrogenase in Chlamydomonas reinhardtii prolongs photo-production of hydrogen from water splitting. *Algal Research* **22**: 116–121.

Nymark M, Valle KC, Brembu T, Hancke K, Winge P, Andresen K, Johnsen G, Bones AM. **2009**. An integrated analysis of molecular acclimation to high light in the marine diatom Phaeodactylum tricornutum. *PLoS ONE* **4**.

O'Brien EJ, Lerman JA, Chang RL, Hyduke DR, Palsson BØ, Adadi R, Volkmer B, Milo R, Heinemann M, Shlomi T. 2013. Genome-scale models of metabolism and gene expression extend and refine growth phenotype prediction. *Molecular systems biology* **9**: 693.

Oakley CA, Hopkinson BM, Schmidt GW. **2012**. A modular system for the measurement of CO_2 and O_2 gas flux and photosynthetic electron transport in microalgae. *Limnology and Oceanography: Methods* **10**: 968–977.

Ohnishi N, Allakhverdiev SI, Takahashi S, Higashi S, Watanabe M, Nishiyama Y, Murata N. **2005**. Two-step mechanism of photodamage to photosystem II: Step 1 occurs at the oxygen-evolving complex and step 2 occurs at the photochemical reaction center. *Biochemistry* **44**: 8494–8499.

Onno Feikema W, Marosvölgyi MA, Lavaud J, van Gorkom HJ. **2006**. Cyclic electron transfer in photosystem II in the marine diatom Phaeodactylum tricornutum. *Biochimica et Biophysica Acta - Bioenergetics* **1757**: 829–834.

Osmond CB. **1981**. Photorespiration and photoinhibition. Some implications for the energetics of photosynthesis. *BBA Reviews On Bioenergetics* **639**: 77–98.

Pan Y, Yang J, Gong Y, Li X, Hu H. **2017**. 3-Hydroxyisobutyryl-CoA hydrolase involved in isoleucine catabolism regulates triacylglycerol accumulation in *Phaeodactylum tricornutum*. *Philosophical Transactions of the Royal Society B: Biological Sciences* **372**: 20160409.

Pedregosa F, Varoquaux G, Gramfort A, Michel V, Thirion B, Grisel O, Blondel M, Prettenhofer P, Weiss R, Dubourg V. 2012. Scikit-learn: Machine Learning in Python. *Journal of Machine Learning Research* **12**: 2825–2830.

Peers G, Truong TB, Ostendorf E, Busch A, Elrad D, Grossman AR, Hippler M, Niyogi KK. **2009**. An ancient light-harvesting protein is critical for the regulation of algal photosynthesis. *Nature* **462**: 518–521.

Peltier G, Cournac L. **2002**. Chlororespiration. *Annual Review of Plant Biology* **53**: 523–550.

Pérez-LLoréns JL, Vergara JJ, Pino RR, Hernández I, Peralta G, Niell FX. **1996**. The effect of photoacclimation on the photosynthetic physiology of ulva curvata and ulva rotundata (ulvales, chlorophyta). *European Journal of Phycology* **31**: 349–359.

Pérez F, Granger BE. **2007**. IPython: A system for interactive scientific computing. *Computing in Science and Engineering* **9**: 21–29.

Peterhansel C, Krause K, Braun H-P, Espie GS, Fernie a R, Hanson DT, Keech O, Maurino VG, Mielewczik M, Sage RF. **2013**. Engineering photorespiration: current state and future possibilities. *Plant biology (Stuttgart, Germany)* **15**: 754–8.

Platt T, Gallegos CL, Harrison WG. **1980**. Photoinibition of photosynthesis in natural assemblages of marine phytoplankton. *Journal of Marine Research (USA)* **38**: 687–701.

Premvardhan L, Robert B, Beer A, Büchel C. **2010**. Pigment organization in fucoxanthin chlorophyll a/c2 proteins (FCP) based on resonance Raman spectroscopy and sequence analysis. *Biochimica et Biophysica Acta - Bioenergetics* **1797**: 1647–1656.

Prihoda J, Tanaka A, De Paula WBM, Allen JF, Tirichine L, Bowler C. **2012**. Chloroplast-mitochondria cross-talk in diatoms. *Journal of Experimental Botany* **63**: 1543–1557.

Raven JA. **2011**. The cost of photoinhibition. *Physiologia Plantarum* **142**: 87–104.

Reinfelder JR. **2011**. Carbon Concentrating Mechanisms in Eukaryotic Marine Phytoplankton. *Annual Review of Marine Science* **3**: 291–315.

Richardson K, Beardall J, Raven J a. **1983a**. Adaption of unicellular algae to irradiance: an analysis of strategies. *New Phytologist* **93**: 157–191.

Richardson K, Beardall J, Raven JA. **1983b**. Adaptation of unicellular algae to irradiance: an analysis of strategies. *New Phytologist* **93**: 157–191.

Ritz M, Thomas J. **2000**. Kinetics of Photoacclimation in Response to a Shift to High Light of the Red Alga. *Society* **123**: 1415–1425.

Rochaix JD. **2011**. Reprint of: Regulation of photosynthetic electron transport. *Biochimica et Biophysica Acta - Bioenergetics* **1807**: 878–886.

Röttgers R. **2007**. Comparison of different variable chlorophyll a fluorescence techniques to determine photosynthetic parameters of natural phytoplankton. *Deep-Sea Research Part I: Oceanographic Research Papers* **54**: 437–451.

Ryther JH. **1956**. Photosynthesis in the Ocean as a Function of Light Intensity. *Limnology and Oceanography* **1**: 61–70.

Saroussi S, Beer S. **2007**. Alpha and quantum yield of aquatic plants derived from PAM fluorometry: Uses and misuses. *Aquatic Botany* **86**: 89–92.

Schaller-Laudel S, Volke D, Redlich M, Kansy M, Hoffmann R, Wilhelm C, Goss R. **2015**. The diadinoxanthin diatoxanthin cycle induces structural rearrangements of the isolated FCP antenna complexes of the pennate diatom Phaeodactylum tricornutum. *Plant Physiology and Biochemistry* **96**: 364–376.

Schellenberger Costa B, Sachse M, Jungandreas A, Bartulos CR, Gruber A, Jakob T, Kroth PG, Wilhelm C. **2013**. Aureochrome 1a Is Involved in the Photoacclimation of the Diatom Phaeodactylum tricornutum. *PLoS ONE* **8**.

Schindelin J, Arganda-Carreras I, Frise E, Kaynig V, Longair M, Pietzsch T, Preibisch S, Rueden C, Saalfeld S, Schmid B. 2012. Fiji: an open-source platform for biological-image analysis. *Nature Methods* **9**: 676–682.

Schmitz J, Srikanth N V., Hüdig M, Poschmann G, Lercher MJ, Maurino VG. **2017**. The

ancestors of diatoms evolved a unique mitochondrial dehydrogenase to oxidize photorespiratory glycolate. *Photosynthesis Research* **132**: 183–196.

Schnitzler Parker M, Armbrust EV, Piovia-Scott J, Keil RG. **2004**. Induction of photorespiration by light in the centric diatom *thalassiosira weissflogii* (bacillariophyceae): molecular characterization and physiological consequences. *Journal of Phycology* **40**: 557–567.

Shikanai T, Yamamoto H. **2017**. Contribution of Cyclic and Pseudo-cyclic Electron Transport to the Formation of Proton Motive Force in Chloroplasts. *Molecular Plant* **10**: 20–29.

Smith SR, Abbriano RM, Hildebrand M. **2012**. Comparative analysis of diatom genomes reveals substantial differences in the organization of carbon partitioning pathways. *Algal Research* **1**: 2–16.

Smith SR, Gillard JTF, Kustka AB, McCrow JP, Badger JH, Zheng H, New AM, Dupont CL, Obata T, Fernie AR. 2016. Transcriptional Orchestration of the Global Cellular Response of a Model Pennate Diatom to Diel Light Cycling under Iron Limitation. *PLoS Genetics* **12**: 1–39.

Soon Chow W, Lee H-Y, Park Y-I, Park Y-M, Hong Y-N, Anderson JM. **2002**. The role of inactive photosystem-II-mediated quenching in a last-ditch community defence against high light stress in vivo. *Philosophical Transactions of the Royal Society B: Biological Sciences* **357**: 1441–1450.

Sosik HM, Mitchell BG. **1991**. Absorption, fluorescence, and quantum yield for growth in nitrogen-limited Dunaliella tertiolecta. *Limnology and Oceanography* **36**: 910–921.

Sosik HM, Mitchell BG. **1994**. Effects of Temperature on Growth, Light Absorption, and Quantum Yield in Dunaliella Tertiolecta (Chlorophyceae). *Journal of Phycology* **30**: 833–840.

Tagawa K, Tsujimoto HY, Arnon DI. **1963**. Role of chloroplast ferredoxin in the energy conversion process of photosynthesis. *Proceedings of the National Academy of Sciences of the United States of America* **49**: 567–572.

Tatusov RL. **2000**. The COG database: a tool for genome-scale analysis of protein functions and evolution. *Nucleic Acids Research* **28**: 33–36.

Tikkanen M, Mekala NR, Aro EM. **2014**. Photosystem II photoinhibition-repair cycle protects Photosystem i from irreversible damage. *Biochimica et Biophysica Acta - Bioenergetics* **1837**: 210–215.

Tsuji Y, Nakajima K, Matsuda Y. **2017**. Molecular aspects of the biophysical CO2-concentrating mechanism and its regulation in marine diatoms. *Journal of Experimental Botany* **68**: 3763–3772.

Tyystjärvi E. **2008**. Photoinhibition of Photosystem II and photodamage of the oxygen evolving manganese cluster. *Coordination Chemistry Reviews* **252**: 361–376.

Tyystjärvi T, Tuominen I, Herranen M, Aro EM, Tyystjärvi E. **2002**. Action spectrum of psbA gene transcription is similar to that of photoinhibition in Synechocystis sp. PCC 6803. *FEBS Letters* **516**: 167–171.

Ueno Y, Aikawa S, Kondo A, Akimoto S. **2016**. Energy Transfer in Cyanobacteria and Red Algae: Confirmation of Spillover in Intact Megacomplexes of Phycobilisome and Both Photosystems. *Journal of Physical Chemistry Letters* **7**: 3567–3571.

Vicente JB, Gomes CM, Wasserfallen A, Teixeira M. **2002**. Module fusion in an A-type flavoprotein from the cyanobacterium Synechocystis condenses a multiple-component pathway in a single polypeptide chain. *Biochemical and Biophysical Research Communications* **294**: 82–87.

Walther G-R, Post E, Convey P, Menzel A, Parmesan C, Beebee TJC, Fromentin J-M, Hoegh-Guldberg O, Bairlein F. **2002**. Ecological responses to recent climate change. *Nature* **416**: 389–395.

Wilhelm C, Jungandreas A, Jakob T, Goss R. **2014**. Light acclimation in diatoms: From phenomenology to mechanisms. *Marine Genomics* **16**: 5–15.

Wolf-Gladrow DA, Zeebe RE, Klaas C, Körtzinger A, Dickson AG. **2007**. Total alkalinity: The explicit conservative expression and its application to biogeochemical processes. *Marine Chemistry* **106**: 287–300.

Yamori W, Shikanai T. **2016**. Physiological Functions of Cyclic Electron Transport Around Photosystem I in Sustaining Photosynthesis and Plant Growth. *Annual Review of Plant Biology* **67**: 81–106.

Zhang B, Horvath S. **2005**. A General Framework for Weighted Gene Co-Expression Network Analysis. *Statistical Applications in Genetics and Molecular Biology* **4**.

Zhu S-H, Green BR. **2010**. Photoprotection in the diatom Thalassiosira pseudonana: role of LI818-like proteins in response to high light stress. *Biochimica et biophysica acta* **1797**: 1449–57.

Zuñiga C, Levering J, Antoniewicz MR, Guarnieri MT, Betenbaugh MJ, Zengler K. **2017**. Predicting dynamic metabolic demands in the photosynthetic eukaryote Chlorella vulgaris. *Plant Physiology*: 17006051–6052017.

Table 4.1. Cellular carbon, nitrogen, chlorophyll a concentrations and variable fluorescence yield measured in wild type (WT) and mutant (LHCX1A) cell lines at low light (LL) control and after 24 hours high light (HL) treated environments.

Sample	C pg/cell	N pg/cell	Chl a pg/cell	C:N	C:Chl	Fv/Fm
WT_LL	11.44 ± 1.45	1.77 ± 0.07	0.58 ± 0.05	6.47 ± 0.46	21.07 ± 1.80	0.72 ± 0.01
WT_HL	15.46 ± 2.10	2.08 ± 0.21	0.21 ± 0.02	7.43 ± 0.68	77.32 ± 6.62	0.59 ± 0.01
LHCX1A_LL	10.98 ± 0.97	1.79 ± 0.50	0.50 ± 0.04	6.12 ± 0.41	22.04 ± 1.57	0.69 ± 0.00
LHCX1A_HL	17.43 ± 0.49	2.17 ± 0.19	0.19 ± 0.01	8.03 ± 0.28	91.26 ± 3.19	0.49 ± 0.02

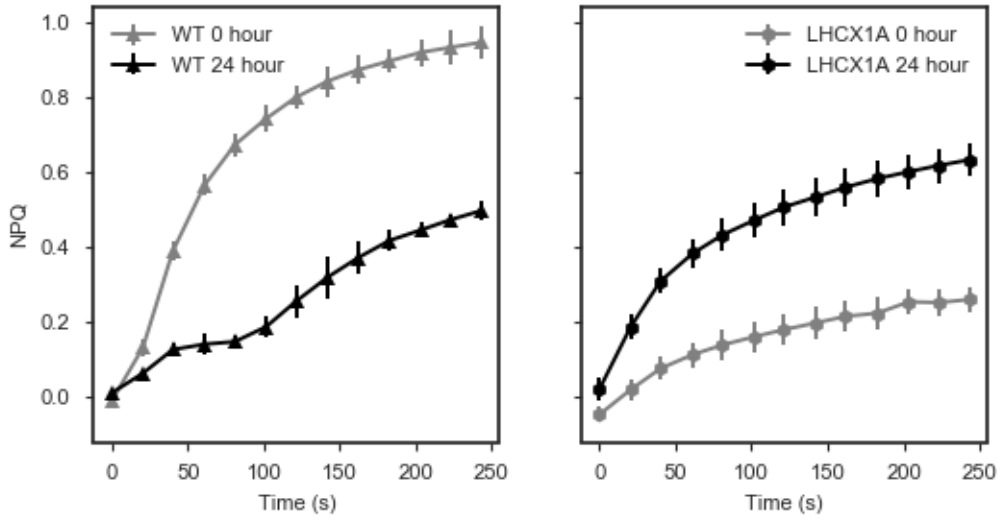

Figure 4.1. NPQ responses of wild type (WT) and mutant (LHCX1A) cell lines at the beginning (0 hour) and the end of 24 hour LL-to-HL acclimation.

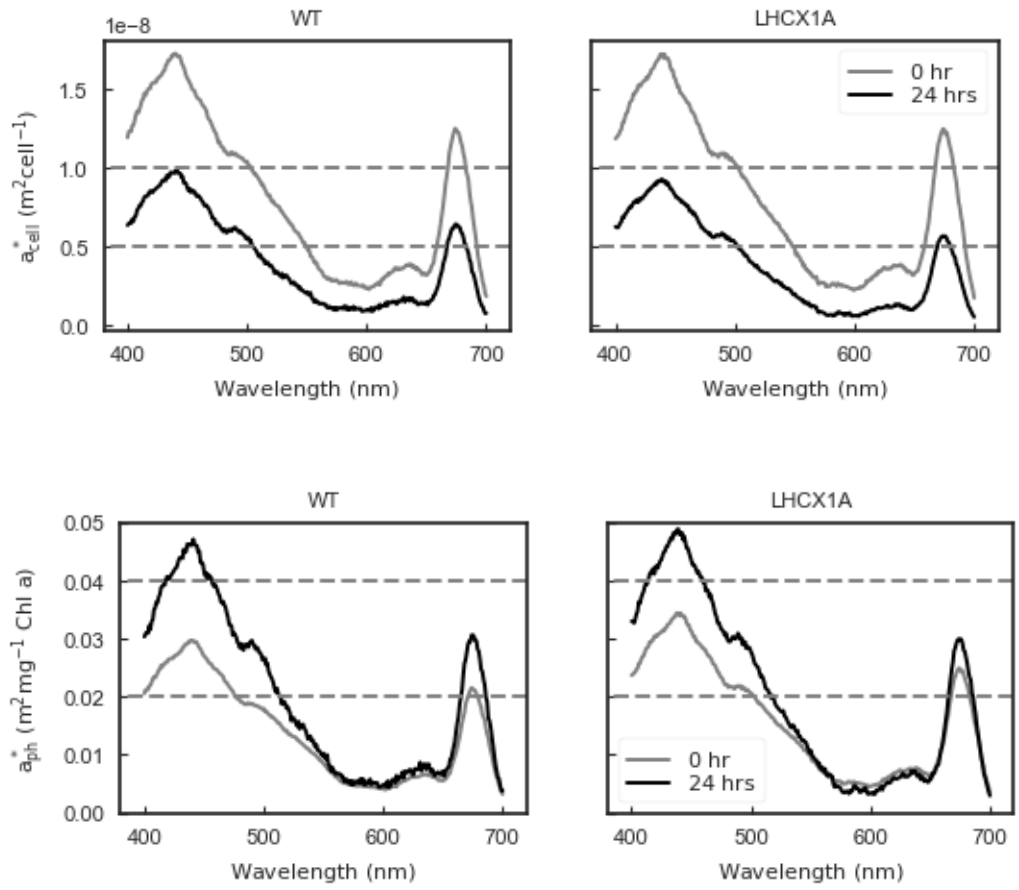

Figure 4.2. Chlorophyll a specific spectral absorption coefficients of WT and LHCX1A culture measured at 0 and 24 hours during the 24 hours LL-to-HL acclimation.

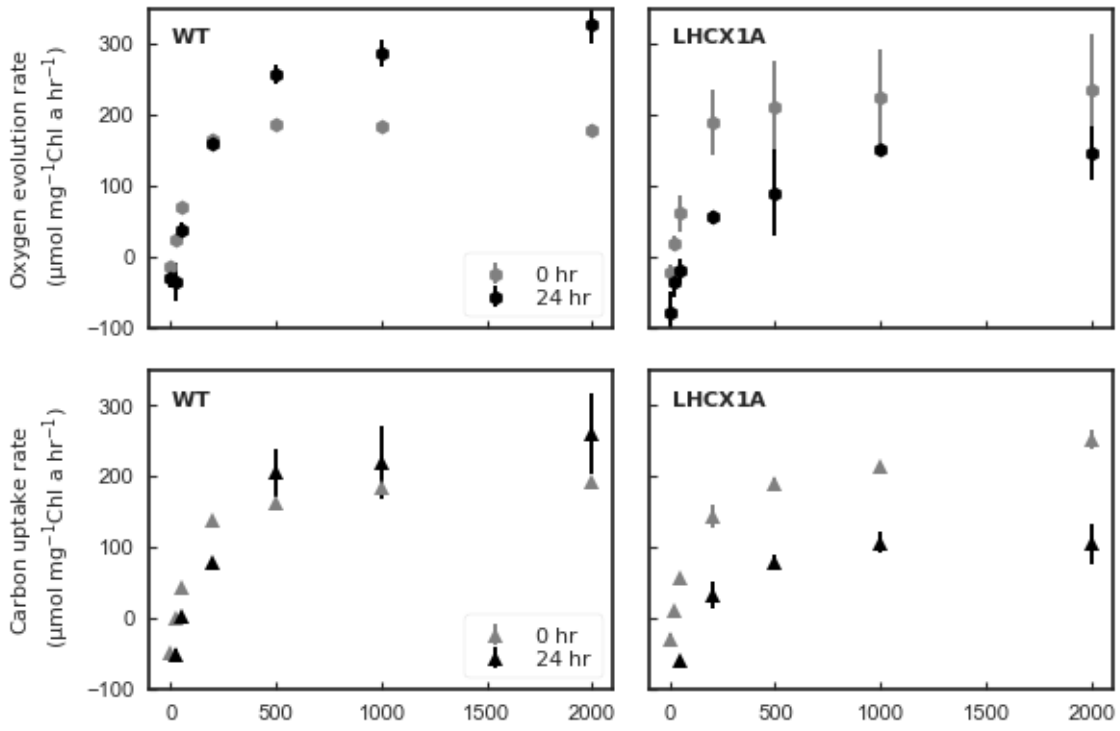

Figure 4.3. Chlorophyll a specific oxygen evolution and carbon uptake P vs. E responses for WT and LHCX1A. The measurement was conducted with pHOS-MIMS system at 0 and 24 hours during the 24 hours LL-to-HL acclimation.

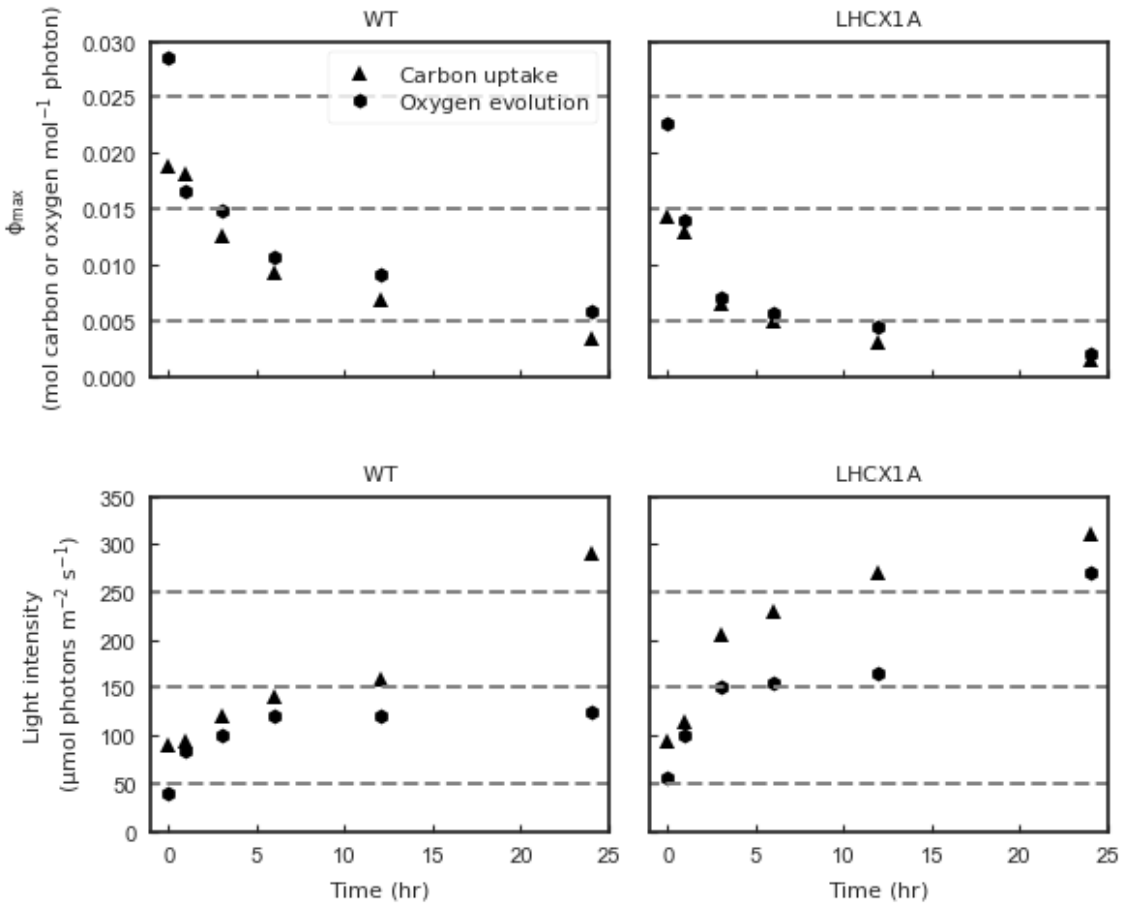

Figure 4.4. Maximal levels of quantum yields Φ_{max} and their corresponding light intensities in WT and LHCX1A lines during the 24 hours LL-to-HL acclimation.

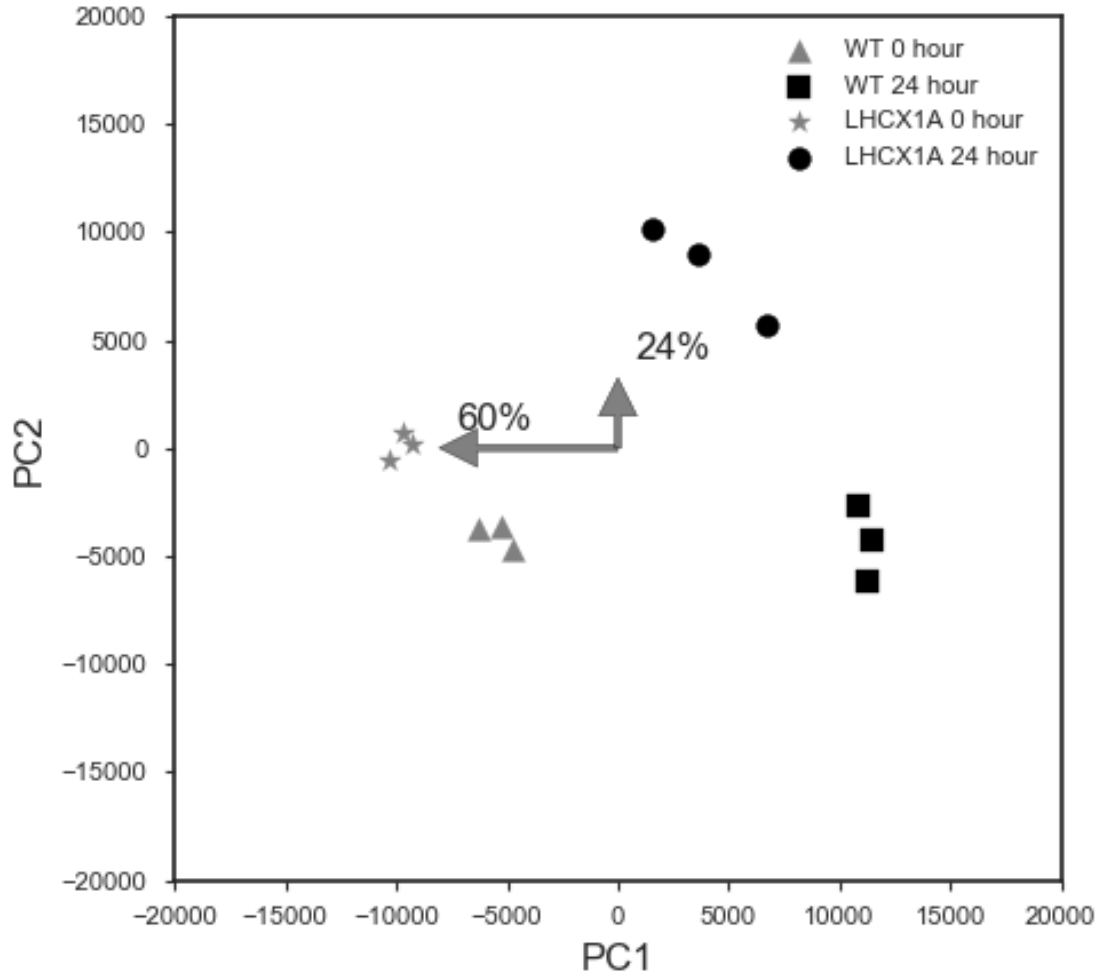

Figure 4.5. PCA graph of triplicated WT and LHCX1A samples plotted in two dimensions using their projections onto the first two principal components. The arrows denote the eigenvectors that describe the relative contribution of each principle component (PC) of the total variance. In this 2 dimension plot only the first 2 PCs are presented.

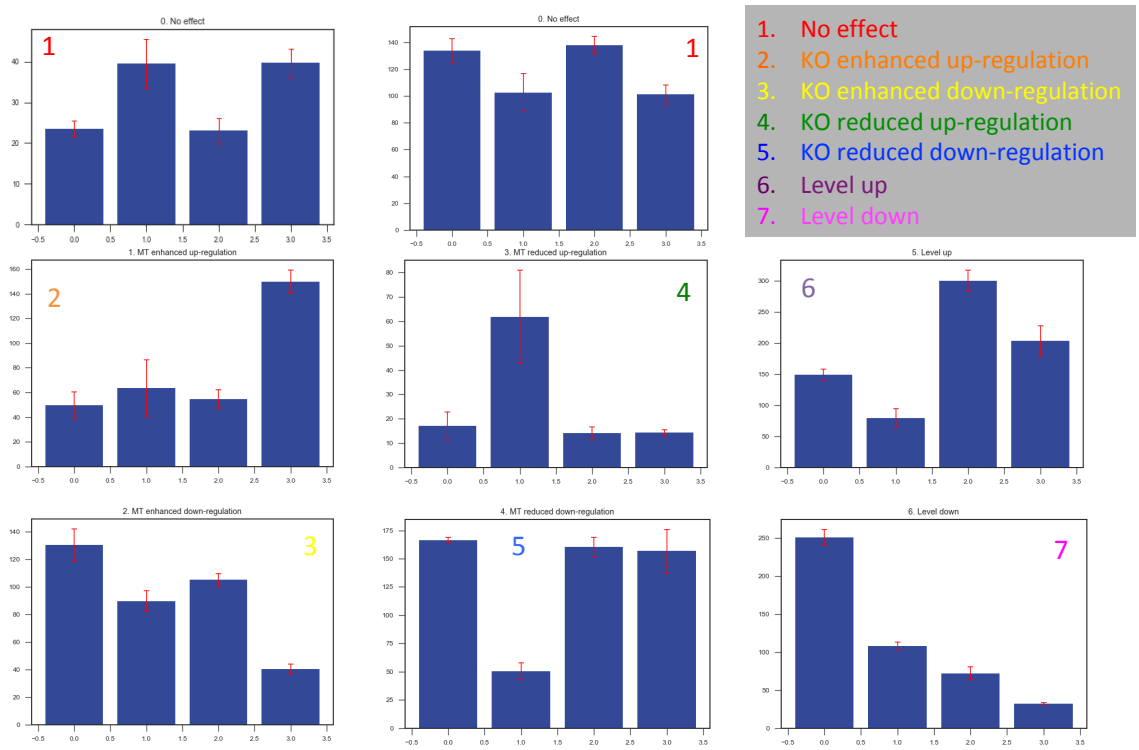

Figure 4.6. Expression categories that represent possible expression types observed in the RNA-Seq data pool. 1. No effect, both wild type (WT) line and LHCX1A knockout line (KO) line exhibited the same level of transcription regulations in response to the HL treatment; 2. KO enhanced up-regulation, an up-regulation trend was found in both the WT and KO, and the magnitude is larger in the KO; 3. KO enhanced down-regulation, a down-regulation trend was found in both the WT and KO, and the magnitude is larger in the KO; 4. KO reduced up-regulation, an up-regulation trend was found in both the WT and KO, and the magnitude is larger in the WT; 5. KO reduced down-regulation, a down-regulation trend was found in both the WT and KO, and the magnitude is larger in the WT; 6. Level up, the overall expression levels are higher in the KO; 7. Level down, the overall expression levels are lower in the KO. The 4 columns from left to right are WT at 0 hour, WT at 24 hour, LHCX1A at 0 hour and LHCX1A at 24 hour.

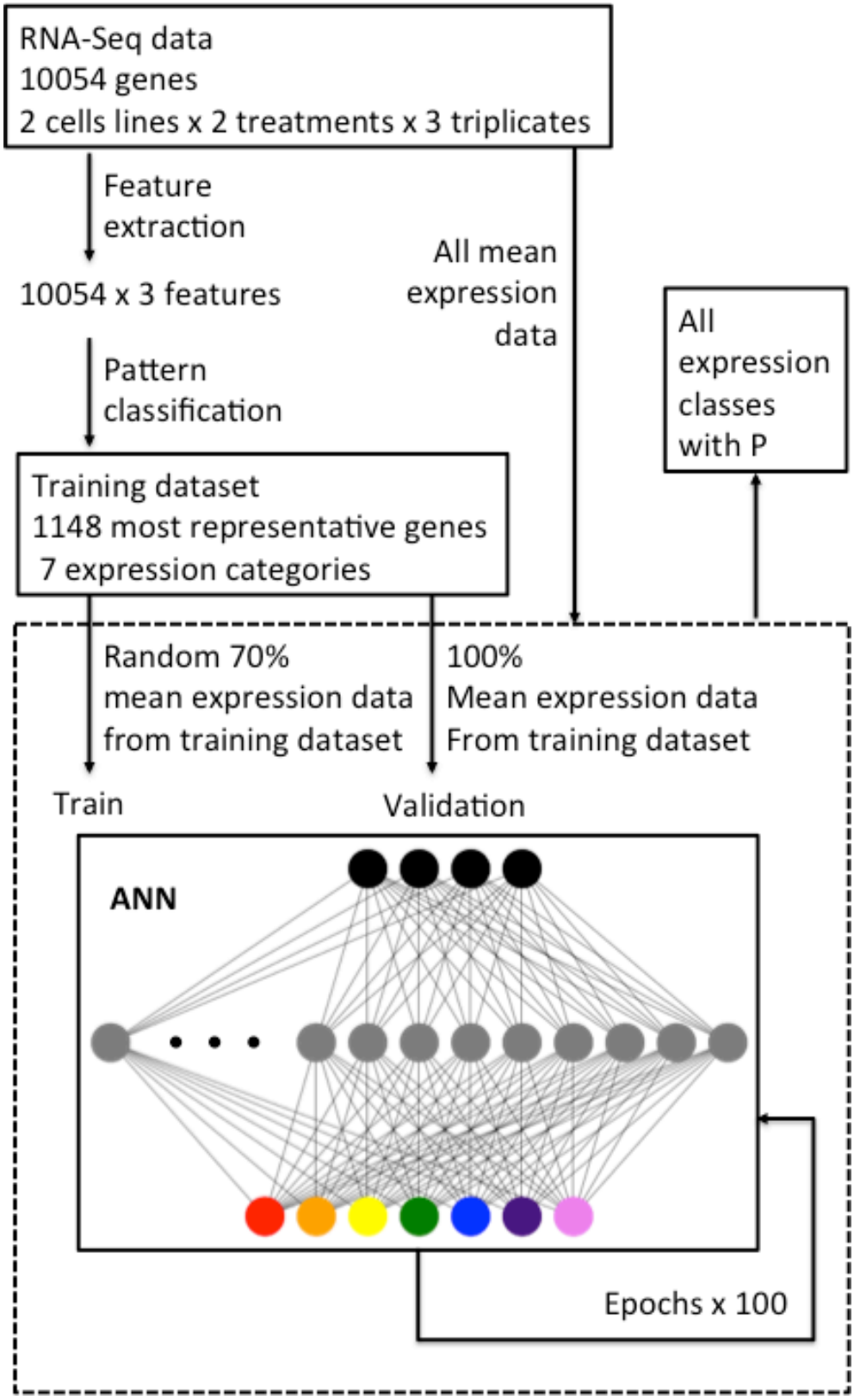

Figure 4.7. Structure and training of the ANN model

Figure 4.8. Gene expression patterns break down by pathways generated from trained ANN model classifier. 'A': 'Amino acid transport and metabolism', 'B': 'Carbohydrate transport and metabolism', 'C': 'Cell cycle control, cell division, chromosome partitioning', 'D': 'Cell wall/membrane/envelope biogenesis', 'E': 'Chromatin structure and dynamics', 'F': 'Coenzyme transport and metabolism', 'G': 'Cytoskeleton', 'H': 'Defense mechanisms', 'I': 'Energy production and conversion', 'J': 'Inorganic ion transport and metabolism', 'K': 'Intracellular trafficking, secretion, and vesicular transport', 'L': 'Lipid transport and metabolism', 'M': 'Nuclear structure', 'N': 'Nucleotide transport and metabolism', 'O': 'Photosynthesis', 'P': 'Posttranslational modification, protein turnover, chaperones', 'Q': 'RNA processing and modification', 'R': 'Replication, recombination and repair', 'S': 'Secondary metabolites biosynthesis, transport and catabolism', 'T': 'Signal transduction mechanisms', 'U': 'Transcription', 'V': 'Translation, ribosomal structure and biogenesis', 'W': 'Unknown', 'X': 'Control'. The color code represent different expression patterns that are defined in Figure 4.6.

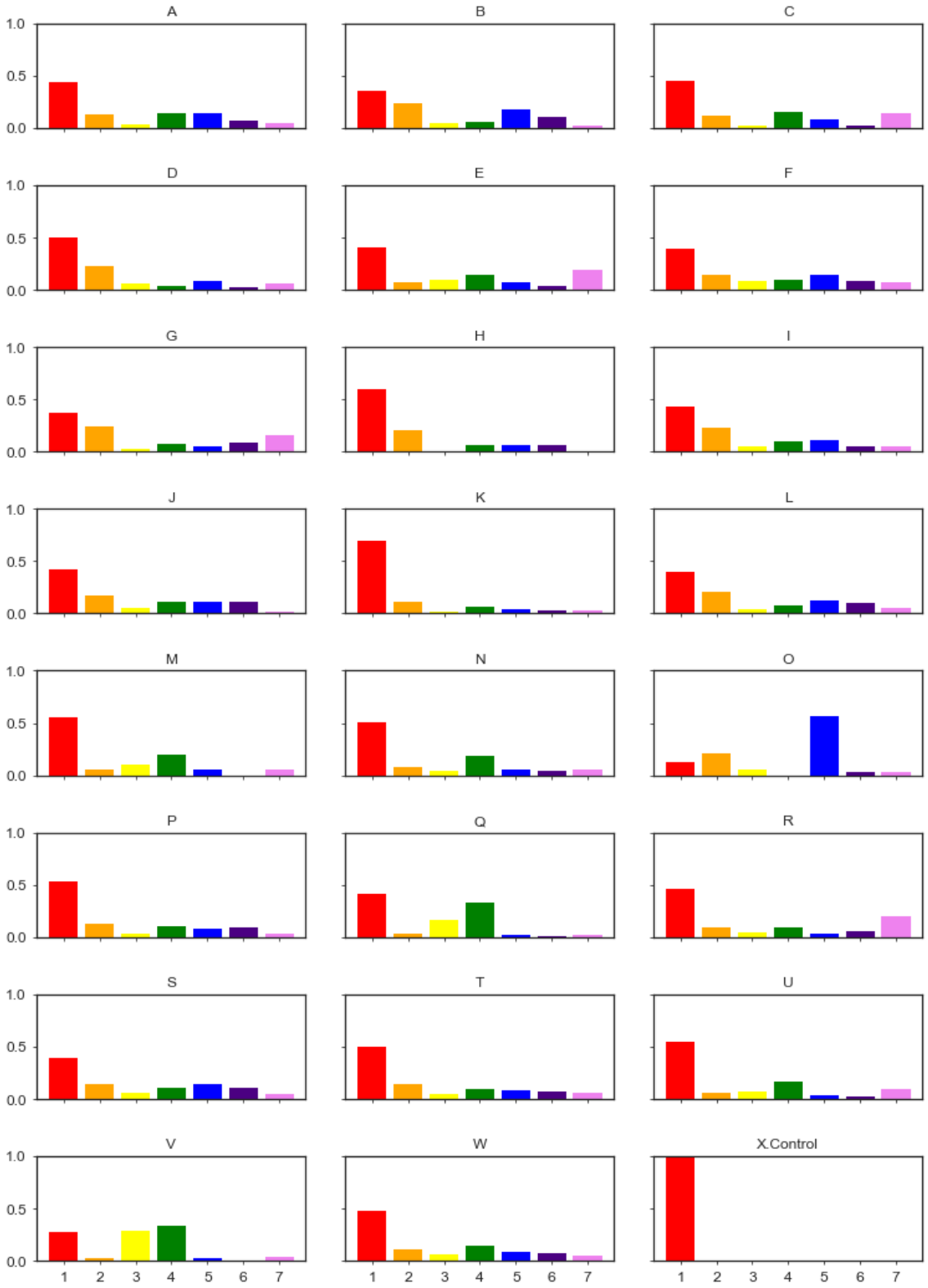
A
B
C
D
E
F
G
H
I
J
K
L
M
N
O
P
Q
R
S
T
U
V
W
X.Control
1.0
0.5
0.0
1 2 3 4 5 6 7

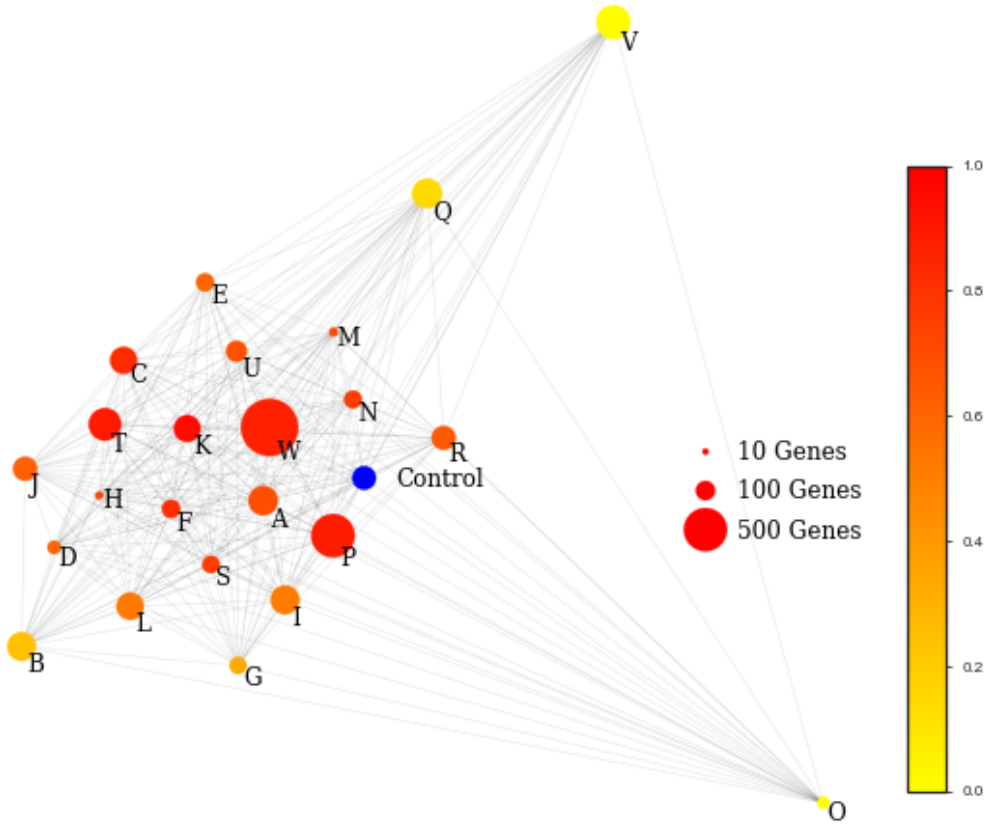

Figure 4.9. Network of *P. tricornuntum* pathway connectivity based on their differential expression patterns during LL to HL acclimation due to LHCX1 gene knockout. The nodes and edges represent the similarity of expression patterns among pathways, and the color gradient shows the similarity between a specific pathway and the control; a higher value of color gradient (more red) indicates a similar pattern of expression. The radius of a node is dictated by the number of valid genes (TPM > 10) within the corresponding pathway.

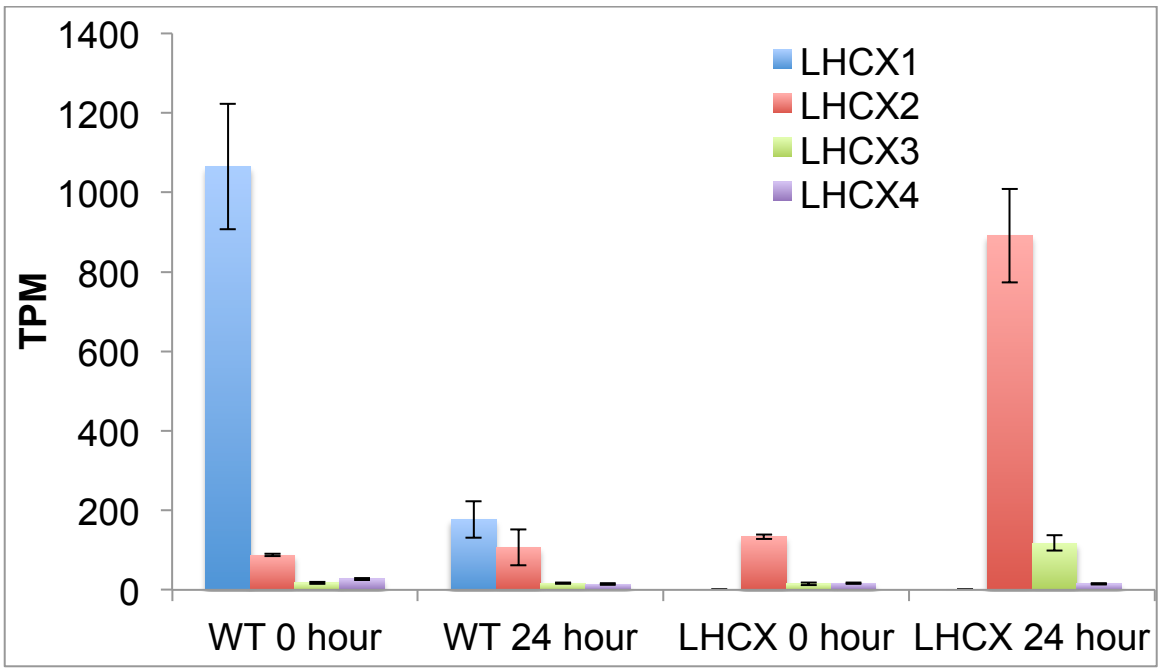

Figure 4.10. Transcript abundances of LHCX gene family in WT and LHCX1A lines before (0 hour) and after 24 hour HL treatment. Error bars show the standard deviation of TPM calculated from raw counts.

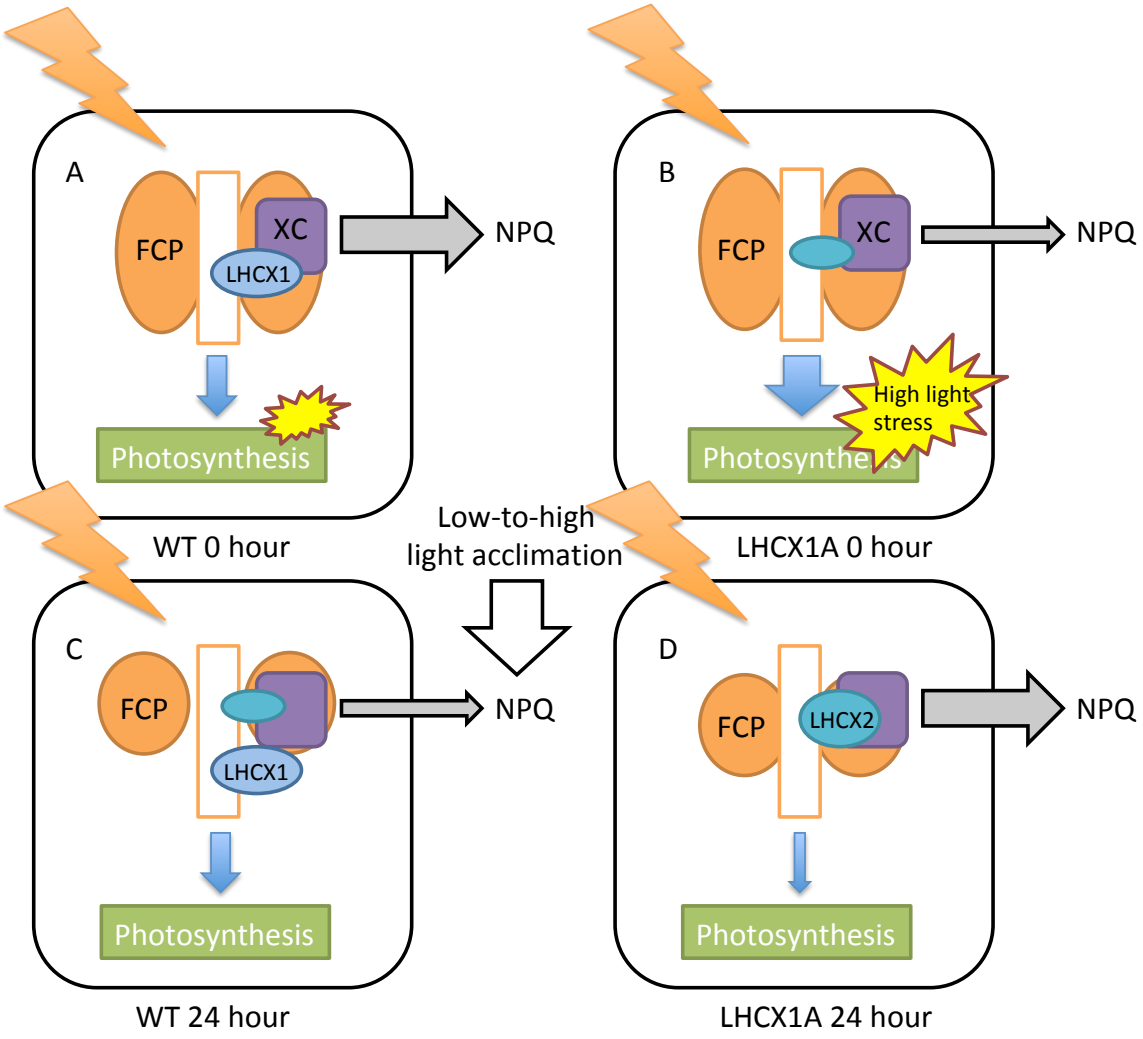

Figure 4.11. Model for the different light utilization in WT and LHCX1A lines before and after 24 hour LL-to-HL acclimation. In LL acclimated cells, upon HL illumination, **A.** FCPC aggregation was quickly induced and LHCX1 functioned with XC de-epoxidation to dissipate NPQ and protect the WT cell from HL stress. **B.** With the absence of LHCX1, the level of LHCX2 transcription was slightly up regulated in the LHCX1A line, however the level of NPQ via LHCX2 and XC de-epoxidation did not provide sufficient photo-protection. After 24 hour LL-to-HL acclimation, **C.** WT cells acclimated to HL and the FCPC aggregation slowed down compare to LL acclimation, therefore the amount of NPQ was minimized to reduce un-necessary energy loss, unless even higher light was applied; **D**. LHCX1A line acclimated to HL rapidly dissipated NPQ regardless of light level due to up regulated LHCX2 expression, resulting in significant energy loss due to NPQ.

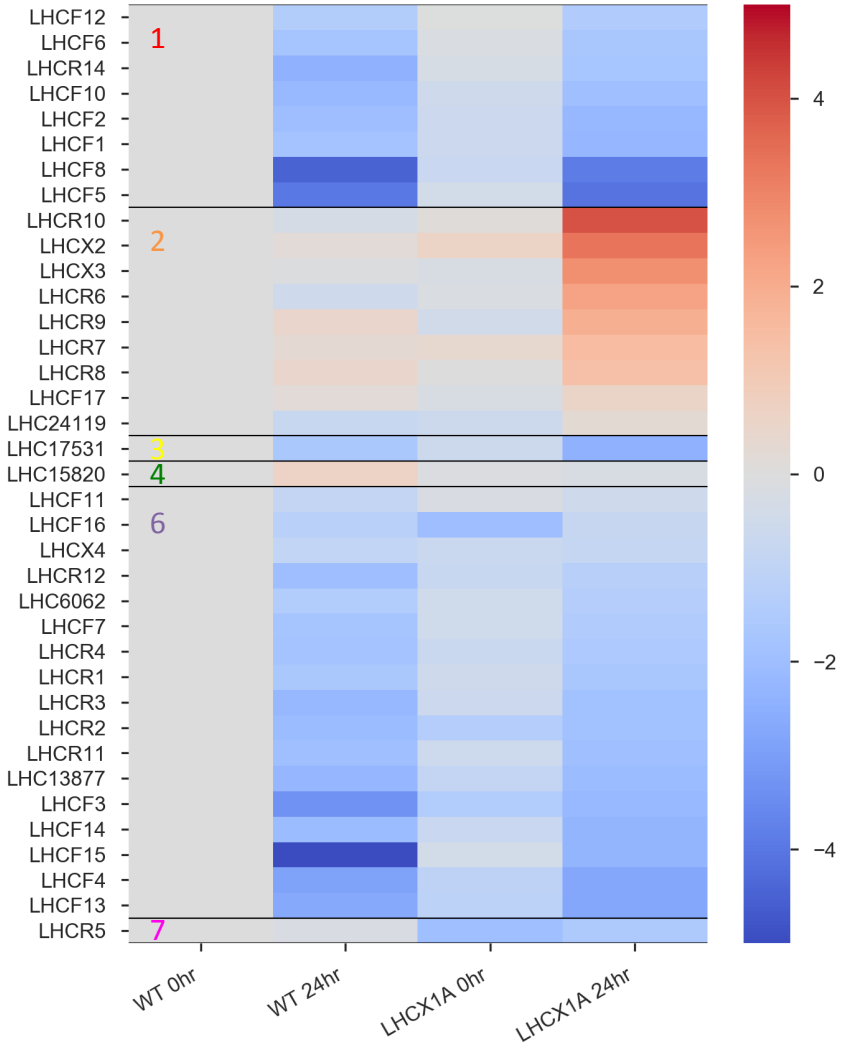

Figure 4.12. Relative transcript expression of light harvesting related genes. Heat map shows RNASeq data as log_2 fold-change in transcript level relative to WT at 0 hour. The abbreviations used are LHCF: major fucoxanthin Chl a/c proteins; LHCR: red algal-like proteins; LHCX: light-harvesting complex stress related protein; LHC#: unclassified light harvesting proteins. The colored numeric IDs indicate the type of gene expression pattern.

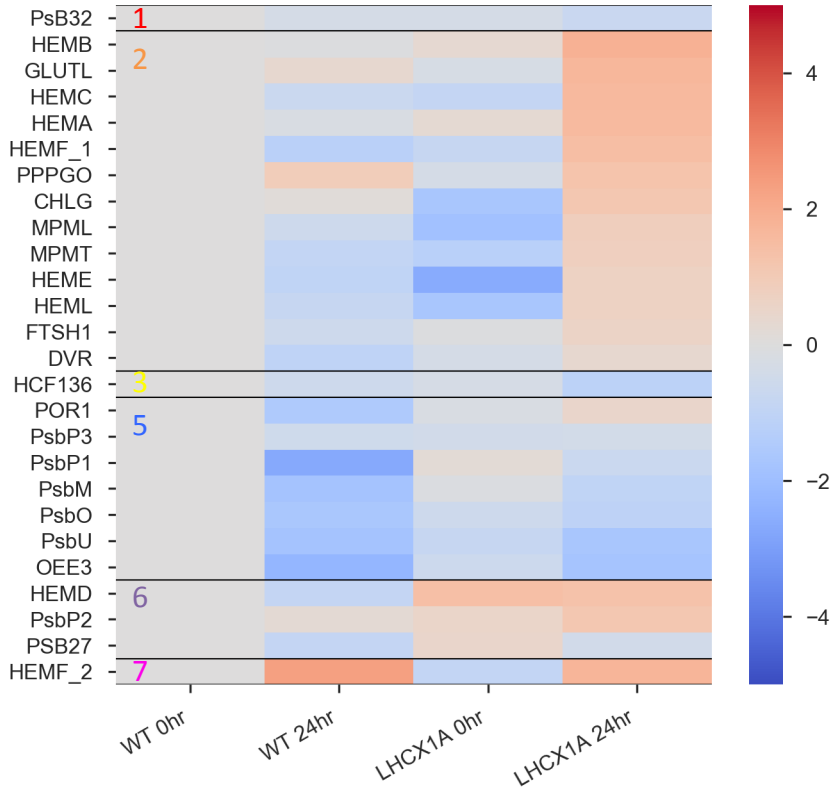

Figure 4.13. Relative transcript expression of PSII and related genes. Heatmap shows RNASeq data as log_2 fold-change in transcript level relative to WT at 0 hour. The abbreviations used are PSB27: Photosystem II Pbs27; PPPGO: Protoporphyrinogen oxidase; POR1: Dehydrogenases with different specificities (related to short-chain alcohol dehydrogenases); MPMT: Methyltransferases; MPML: Protoporphyrin IX magnesium chelatase, subunit D; HEML: Acetylornithine aminotransferase; HEMF_2: Coproporphyrinogen III oxidase CPO/HEM13; HEMF_1: Coproporphyrinogen III oxidase CPO/HEM13; HEME: Uroporphyrinogen decarboxylase; HEMD: Uroporphyrinogen-III synthase HemD; HEMC: Porphobilinogen deaminase; HEMB: Delta-aminolevulinic acid dehydratase; HEMA: Glutamyl-tRNAGlu reductase, dimerisation domain||Shikimate / quinate 5-dehydrogenase||Glutamyl-tRNAGlu reductase, N-terminal domain; HCF136: Sortilin and related receptors; GLUTL: Glutamyl-tRNA synthetase (mitochondrial); FTSH1: AAA+-type ATPase containing the peptidase M41 domain; DVR: Predicted dehydrogenase; CHLG: chlorophyll synthase ChlG; PsbP1: calcium ion binding; PsB32: TLP18.3, Psb32 and MOLO-1 founding proteins of phosphatase; PsbM: Photosystem II reaction centre M protein; PsbP2: calcium ion binding; PsbP3: calcium ion binding; PsbU: Photosystem II 12 kDa extrinsic protein; OEE3: Oxygen evolving enhancer protein 3; PsbO: Manganese-stabilising protein / photosystem II polypeptide; The colored numeric IDs indicate the type of gene expression pattern.